Waveforms MOdels for Machine Type CommuNication inteGrating 5G Networks

(WONG5)

Document Number D4.1

MIMO schemes and associated receivers (preliminary)

Contractual date of delivery:	12/01/2017
Project Number and Acronym:	ANR-15-CE25-0005, WONG5
Editor:	Pascal Chevalier (CNAM)
Authors:	*Jean-Baptiste Dore (CEA), David Demmer (CEA), Pascal Chevalier (TCS), Anne Ferréol (TCS), Rostom Zakaria (CNAM), Didier Le Ruyet (CNAM)*
Participants:	CNAM, TCS, CEA, CS
Workpackage:	WP4
Security:	Public(PU)
Nature:	Report
Version:	0.0
Total Number of Pages:	61

Abstract:

This report is the first deliverable related to WP4 entitled *Benefits of MIMO techniques to decrease latency*. It takes into account the selected waveforms for MTC presented in D2.1 (critical and comparative performance analysis of filtered multi-carrier waveforms), and presents the state of art and preliminary MIMO schemes adapted to the selected waveforms.

Keywords: MIMO, FBMC OQAM, ML, V-Blast, Alamouti, widely linear

Document Revision History

Version	Date	Author	Summary of main changes
0.0	06.12.2016	Pascal Chevalier	Initial structure of the document
0.1	14.03.2017	Jean Baptiste Dore	Latex template
0.2	24.03.2017	Rostom Zakaria	CNAM contributions
0.3	31.03.2017	Anne Ferréol	Contributions and modifications
0.4	25.04.2017	Rostom Zakaria	Corrections and modifications
0.5	10.05.2017	Anne Ferréol	Corrections and modifications

Executive Summary

The goals of the WONG5 project are to study and propose the most appropriate waveforms that are adapted to critical machine type communications. The derived waveforms will be used for the definition of a new physical layer adapted to this context. Deliverable D4.1 describes the state of art and preliminary MIMO schemes adapted to the waveforms which have been selected in WP2 and presented in D2.1.

Table of Contents

1 Introduction **6**
1.1 Context . . . 6
1.2 Objectives . . . 6
1.3 Organization of the report . . . 6

2 Selected waveforms for Machine Type Communications **7**
2.1 WF with complex orthogonality . . . 7
2.1.1 CP-based: OFDM, WOLA, BF-OFDM and FFT-FBMC . . . 7
2.1.2 ZP-based: UFMC (UF-OFDM) . . . 11
2.2 WF with real orthogonality: FBMC-OQAM . . . 12
2.3 WF without orthogonality: FBMC-QAM . . . 13

3 MIMO Technologies **14**
3.1 Overview . . . 14
3.1.1 Presentation and interests . . . 14
3.1.2 MIMO schemes . . . 14
3.2 Coupling of MIMO technology with MC waveforms . . . 14
3.2.1 MIMO for OFDM waveforms . . . 14
3.2.2 MIMO for filtered MC waveforms . . . 15

4 MIMO for filtered waveforms **16**
4.1 WF with complex orthogonality or near complex orthogonality . . . 16
4.1.1 Alamouti . . . 16
4.1.2 Spatial-Multiplexing V-Blast . . . 19
4.2 WF with real orthogonality: state of the art . . . 19
4.2.1 Spatial multiplexing schemes . . . 20
4.2.2 Spatial diversity schemes . . . 25
4.2.3 Principal limitations of existing solutions . . . 31
4.3 WF without orthogonality: state of the art . . . 31
4.3.1 Spatial multiplexing . . . 31
4.3.2 Space-time block coding . . . 32

5 New MIMO tranceiver schemes for filtered waveforms **34**
5.1 Carrier per Carrier processing . . . 34
5.1.1 ML with 3 sub-carriers . . . 34
5.1.2 Alternative ML . . . 42
5.1.3 Joint SIC and MMSE/ZF . . . 42
5.2 Widely Linear processing . . . 43
5.3 Frequency-Spreading detectors . . . 43
5.3.1 Introduction . . . 43
5.3.2 Soft-Decision Linear Receivers for Spatial-Multiplexing FBMC/OQAM with Frequency Spreading receiver . . . 43
5.3.3 Alamouti coding with FBMC/OQAM combined with Frequency Spreading receiver . . . 52
5.4 Multi-Carriers approaches with linear receivers . . . 53

6 References **55**

1. Introduction

1.1 Context

The objective of the WONG5 project is to study and propose the most appropriate post OFDM waveform (WF) for critical machine type communications C-MTC.

Requirements for C-MTC systems have been described in deliverable D1.1 and can be summarized as follows: low latencies, very high reliability and data integrity, high energy efficiency for mobile systems and resistance to asynchronous users (time and frequency).

Based on these requirements, a comparative analysis of available post-OFDM WF has been done in the deliverable D2.1. The output of the comparison corresponds to a restricted set of possible candidates WFs for C-MTC. These WFs will be further studied in WONG5 project.

In task 2.2, studies will be conducted in order to enhance their properties related to C-MTC context. In task 3, energy efficiency improvement will be studied together with their adaptation to analog RF components. During task 4, adaptation of candidate WFs to MIMO systems will be developed.

1.2 Objectives

The objectives of this deliverable D4.1, the first deliverable related to WP4 entitled "Benefits of MIMO technics to decrease latency", is to take into account the selected waveforms for MTC presented in D2.1 (critical and comparative performance analysis of filtered multi-carrier waveforms), and to present the state of art and preliminary MIMO schemes adapted to these selected waveforms. The selected waveforms belong to three families of waveforms:

- The waveforms which are orthogonal in the complex domain : WOLA-OFDM, F-OFDM, FFT-FBMC, BF-OFDM, UFMC
- The waveforms which are orthogonal in the real domain : FBMC-OQAM
- The non-orthogonal waveforms : FBMC-QAM

For latency reasons, the considered MIMO schemes are open-loop schemes, which do not take into account any Channel State Information at Transmission (CSIT). These schemes implement either Spatio-Temporal Coding or Spatial Multiplexing at transmission.

1.3 Organization of the report

The selected waveforms are recalled in Section 2. Section 3 presents the MIMO technology jointly with the selected MIMO schemes. Section 4 presents a critical analysis of the state of art related to the coupling of MIMO schemes with the selected filtered multi-carrier waveforms. Section 5 proposes and analyses several preliminary MIMO solutions for the selected waveforms. Finally section 6 concludes this report.

2. Selected waveforms for Machine Type Communications

2.1 WF with complex orthogonality

2.1.1 CP-based: OFDM, WOLA, BF-OFDM and FFT-FBMC

2.1.1.1 CP-OFDM

CP-OFDM is the most well documented multicarrier waveform. It is widely used in several wireless standards (e.g. IEEE 802.11. a/g/n and 3GPP-LTE). It consists of splitting up of a stream of complex symbols at high-rate into several lower-rate streams transmitted on a set of orthogonal subcarriers which are implemented using the inverse fast Fourier transform (IFFT). The OFDM receiver can be implemented using the fast Fourier transform (FFT). In order to keep the orthogonality between subcarriers, a cyclic prefix (CP) is usually inserted transforming thus the linear channel convolution into circular convolution if the CP is longer than the channel impulse response. Therefore, after the FFT operation, the channel equalization becomes trivial through a single coefficient per subcarrier.

2.1.1.2 WOLA-OFDM

The weighted overlap and add (WOLA) could be applied to CP-OFDM to obtain WOLA-OFDM. WOLA was initially introduced in [Qua] by Qualcomm Incorporated and has been studied in [ZMSR16] with OFDM in asynchronous 5G scenario.

In the WOLA transmitter process, a time domain windowing operation is performed producing thus soft edges at the beginning and the end of original transmitted block. These soft edges are added to the cyclic extension of the OFDM symbol of length $N_s = N$. Indeed, the smooth transition between the last sample of a given symbol and the first sample of the next symbol is provided with point-to-point multiplication of the windowing function and the symbol with cyclic prefix and cyclic suffix. The samples corresponding to CP (of size CP) from the last part of a given symbol are copied and appended to its beginning. Besides, the first W_{Tx} samples of the symbol are added to the end, corresponding to the cyclic suffix. Thus, the WOLA-OFDM time domain symbols are cyclically extended from N_s samples to $N_s + CP + W_{Tx}$.

After the cyclic extensions insertion, a window of length $L = N_s + CP + W_{Tx}$ samples is applied. In fact, many windowing functions have been studied and compared [BT07]. In addition to the transmit windowing, which is used to improve the spectral confinement of the transmitted signal, the WOLA processing is also applied at the receiver side in order to enhance asynchronous inter-user interference suppression. Note that the applied receive window is independent of the transmit one and its length is equal to $N_s + 2W_{Rx}$. This windowing is followed by Overlap and Add processing which minimizes the effects of windowing on the useful data.It is worth emphasizing that the first window part $[0, 2W_{Rx}]$ applied at the receiver must be symmetrical w.r.t the point $(W_{Rx}, \frac{1}{2})$, in order to correctly recover the weighted samples.

2.1.1.3 f-OFDM

Filtered-OFDM (f-OFDM) has been recently proposed as a 5G candidate at the 3GPP RAN1 workgroup [AJM15, HiS16]. This scheme is based on traditional CP-OFDM and follows a pragmatic approach to overcome problems raised by the use of asynchronous communications for which traditional CP-OFDM is known to provide poor performance:

- At the transmission, the poor out-of-band radiation of traditional CP-OFDM is improved using a filter at the output of a CP-OFDM transmitter,
- At the reception, the interferences coming from time and frequency asynchronous adjacent users are lowered thanks to the filtering (signal of interest is supposed to be centered at 0 Hz) at the input of a CP-OFDM receiver.

The advantage of f-OFDM is to keep traditional CP-OFDM as its core waveform at both transmission and reception. All existing and already developed OFDM-based designs are applicable to f-OFDM such as MIMO, channel estimation/equalization, pilot, synchronization, PAPR reduction (DFT precoding or any others approaches). In addition, an important advantage of f-OFDM is to enable the co-existence of different time-frequency granularities (i.e. numerologies), such as different subcarrier spacings, cyclic prefix sizes, burst lengths, ...

The filtering process required by the f-OFDM scheme introduces some drawbacks such as complexity, potential inter block interference and an increase of the burst length and consequently an increase of the latency.

2.1.1.4 FFT-FBMC

In order to overcome the FBMC intrinsic interference issue, FFT-FBMC scheme, together with a special data transmission strategy has been proposed in [ZR12, ZLR10a]. This scheme proceeds by precoding the data in a subcarrier-wise manner using an IFFT. Thus, the interference coming from the same subcarrier is removed by a simple equalization thanks to the subcarrier-wise IFFT/FFT precoding/decoding and cyclic prefix (CP) insertion. Whereas the interference coming from the adjacent subcarriers can be avoided by a special data transmission strategy and a good frequency-localized prototype filter.

In FFT-FBMC proposal, blocks of $N/2$ data complex symbols in each subcarrier k go through a N-IFFT operation. The $N/2$ data symbols are alternately fed to the first and last $N/2$ bins of the N-IFFT. When the subcarrier index k is odd (resp. even), the symbols are fed to the first (resp. last) $N/2$ bins. After that, the N-IFFT outputs are extended with a cyclic prefix (CP) of size L, and fed to the FBMC modulator in a given subcarrier k. Fig. 2-1 depicts the scheme of the FFT-FBMC proposed in [ZLR10a]. Let us denote by $d_{k,p}[l]$ the l-th complex data symbol in the p-th block to be transmitted in the k-th subcarrier. According to the FFT-FBMC scheme developed in [ZR12], the symbols $a_{k,n}$ at the input of the FBMC modulator can be written as:

$$a_k[n] = \frac{e^{j\pi n(k+1)}}{\sqrt{N}} \sum_{l=0}^{\frac{N}{2}-1} d_{k,p}[l] e^{j\frac{2\pi nl}{N}} \tag{2.1}$$

where p is the block index given by $p = \left\lceil \frac{n}{N+L} \right\rceil + 1$. It is worth noticing that the first exponential term in the equation above is related to the alternating rule mentioned in the beginning of this section.

At the output of the FBMC demodulator, the serial symbols $z_q[n]$ in each subcarrier q are reshaped into blocks of size $N + L$ to only keep N symbols in each block. This operation is referred to as "S/P + CP removal" in Fig. 2-2. After that, N symbols of each block p' are fed to a N-FFT whose only $N/2$ output symbols are kept for detection. Again, the first $N/2$ output symbols are kept when the subcarrier index q is odd, and the last $N/2$ symbols are

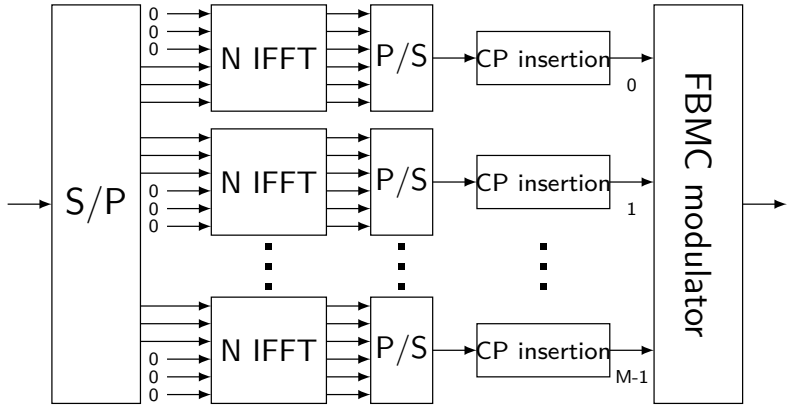

Figure 2-1: FFT-FBMC transmitter scheme

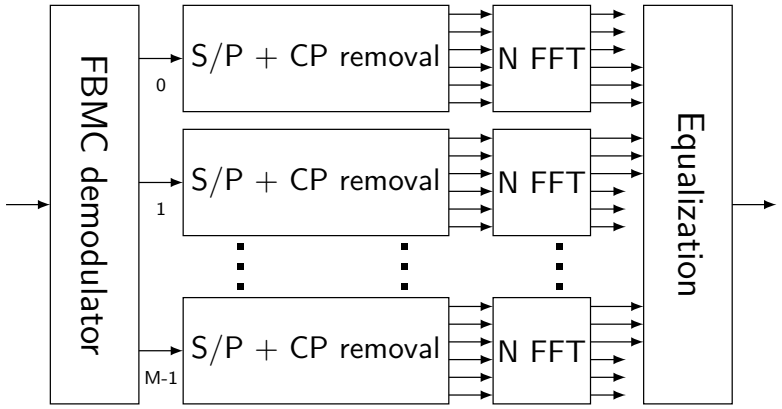

Figure 2-2: FFT-FBMC receiver scheme

kept when q is even. Fig. 2-2 depicts the overall scheme of FFT-FBMC receiver. Therefore, the FFT-FBMC demodulated symbols (just before Equalization block) can be expressed as:

$$x_{q,p'}[l'] = \frac{1}{\sqrt{N}} \sum_{n \in B_{p'}} e^{-j\pi n(q+1)} z_q[n] e^{-j\frac{2\pi n l'}{N}} \quad \text{for} \quad l' \in \left\{0, ..., \frac{N}{2} - 1\right\} \tag{2.2}$$

where $B_{p'} = \left\{(p'-1)(N+L) + L/2, ..., p'(N+L) - L/2 - 1\right\}$. We note again that the first exponential term in the equation above is related to the alternating rule concerning the $N/2$ kept symbols for detection in each subcarrier q.

$$x_{q,p'}[l'] = \tilde{H}_q[l'] d_{q,p'}[l'] + \tilde{w}_{q,p'}[l'] \tag{2.3}$$

where $\tilde{w}_{q,p'}[l']$ is the noise term, and $\tilde{H}_q[l']$ is the equivalent channel coefficient given by [ZR16]

$$\tilde{H}_q[l'] = H\left[l' + q\frac{N}{2}\right] \times F\left[l'\right] \quad \text{for } l' \in \left\{-\frac{N}{4}, ..., \frac{N}{4} - 1\right\} \tag{2.4}$$

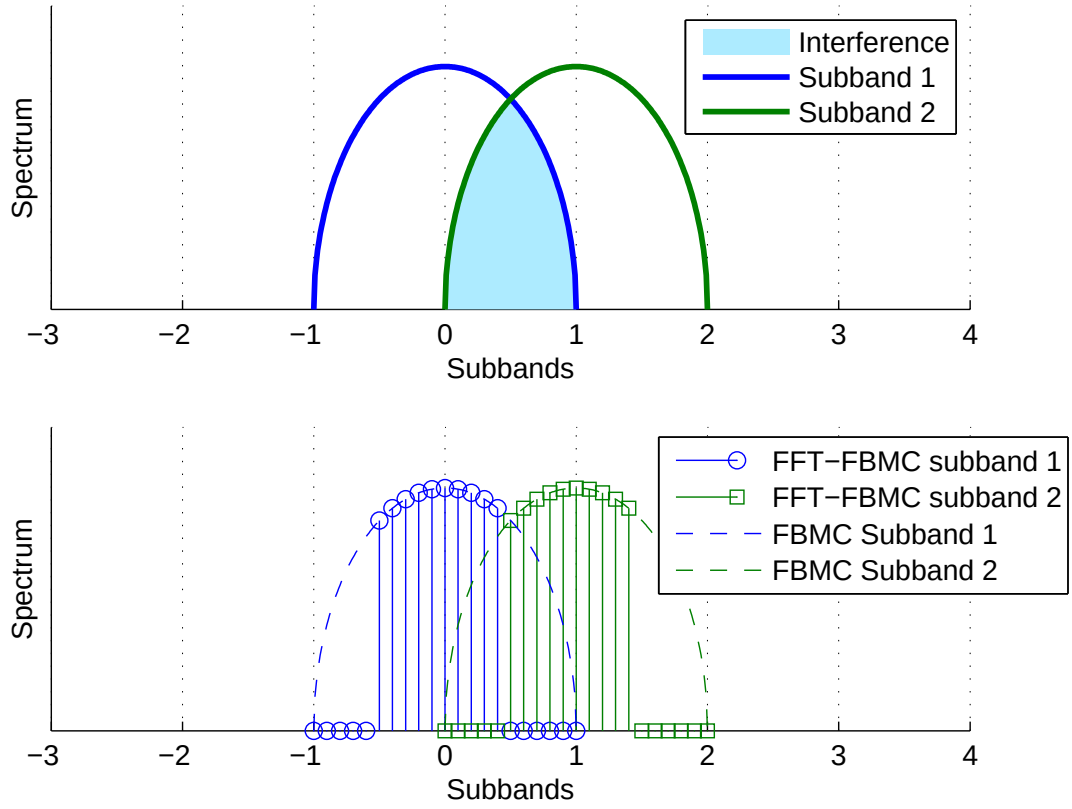

Figure 2-3: Illustration of the complex orthogonality in FFT-FBMC.

with $H[\mu] = \sum_\tau h[\tau] e^{-j\frac{4\pi}{MN}\mu\tau}$ denotes the discrete frequency response of the channel $h[\tau]$ at tones $\frac{2\mu}{MN}$, and where $F[l]$ is the discrete Fourier transform (DFT) of the downsampled by $M/2$ of the prototype filter autocorrelation.

Therefore, one can observe that according to (2.3) the complex orthogonality is restored in FFT-FBMC. The intercarrier interference is avoided thanks to the $N/2$ zeros inserted in the N-IFFT in each subband. For the sake of clarity and illustration, Fig 2-3 depicts in a qualitative manner the spectrum of two active adjacent subcarriers in FBMC and FFT-FBMC. The first plot shows that ICI in FBMC is generated due to the overlapping of both filter frequency responses. Whereas, we show for FFT-FBMC in the second plot that each subband is devided into N smaller subbands where only the $N/2$ middle ones are active. This corresponds to the $N/2$ nonzero symbols at the input of the N-IFFT in each subcarrier. That is, the $N/2$ zeros inserted in each N-IFFT serve to isolate the adjacent subbands. It is worth noticing that normally, in Fig. 2-1, the $N/2$ zeros should be in the middle of each N-IFFT. However, since the "FBMC modulator" introduces a phase rotation of $\Phi_k[n] = e^{j\frac{\pi}{2}(k+n)-j\pi kn}$ [ZR12], the zero positions are changed accordingly.

2.1.1.5 BF-OFDM

Block-Filtered OFDM (BF-OFDM) is a precoded filter-bank multi-carrier modulation [DGD+17] [GDDK17]. The precoding scheme is performed by means of Inverse Fourier Transforms (IFTs) and Cyclic Prefix (CP) insertion, hence the name of the modulation scheme. The idea of such precoding was first proposed in [ZR12] and is detailed in previous sub section. It aims at highly

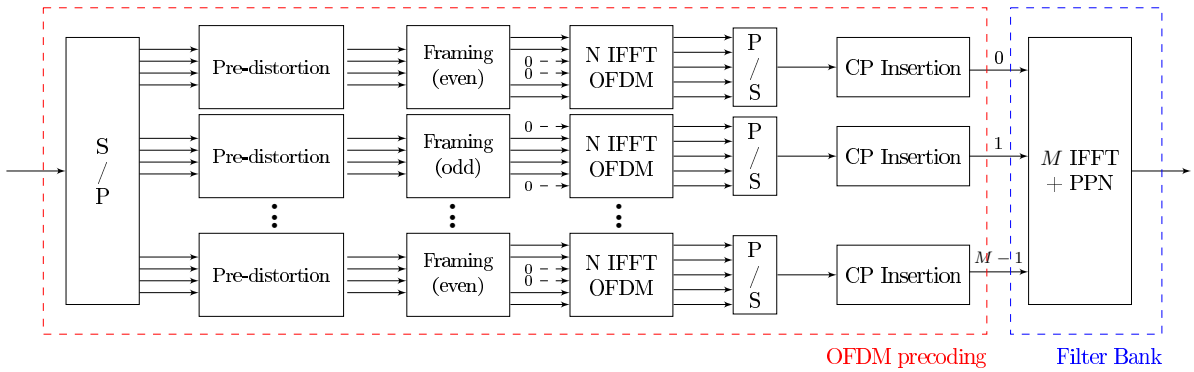

Figure 2-4: BF-OFDM transmitter scheme.

attenuating the filter-bank inherent interferences but leads to a complex receiver structure composed of a synthesis filter bank concatenated with CP-OFDM demodulators. BF-OFDM can be seen as an improved version of FFT-FBMC. The key idea is to prepend a pre-distortion stage to the transmitter chain in order to rely on a low-complex CP-OFDM like receiver.

The transmitter and receiver schemes are respectively depicted in figures 2-4 and 2-5. The transmitter is thus composed of a precoding stage followed by a filter bank. Regarding the precoding, the pre-distortion stage compensates the distortion induced by filter bank (in both amplitude and phase) in order to flatten the received signal spectrum inside the carrier bandwidth at the receiver side. Then, the framing maps the $N/2$ active subcarriers for each carrier. The subcarrier allocation depends on the carrier index (its parity) and ensures the perfect complex orthogonality at the carrier level [DGD+17]. Finally, there are the CP-OFDM modulators. Indeed, a CP insertion is required in order to preserve the circularity of the signal, so as in legacy CP-OFDM. The filtering is operated by means of a M-point IFFTs and a PolyPhase-Network (PPN). As the symbols are spread in time because of the PPN (with an overlapping factor equal to K), an overlapping stage is considered at the end of the transmission chain in order to improve the Spectral Efficiency (SE). However the overlapping generates Inter-Symbol Interferences (ISI) as neighbour symbols in time are captured with the useful one. To come up with it, the CP length must be greater or equal than $2K-1$ [DGD+17]. This condition on the CP length leads to a significant loss of SE therefore in practice shorter CP are used at the expense of a Signal-to-Interference Ratio (SIR) penalty. The common choice is to set the CP length so that the SE is equivalent to the legacy CP-OFDM.

The receiver is simply composed of a $\frac{MN}{2}$-point FFT and is therefore highly similar to the receiver used in conventional OFDM. No filtering stage are required thanks to the predistortion stage that is added at the transmitter side.

BF-OFDM is said to be complex-orthogonal but rigorously it is not. Indeed even if a perfect orthogonality is satisfied at the carrier level by the framing, inter-carrier interferences are generated by the filter bank. However, the rejection of those interferences are controlled by both the filter shape and the CP and provides SIR of about 60 dB. Such a SIR level does not disturb the transmission over the other carriers and that is why the modulation scheme is said to be complex orthogonal.

2.1.2 ZP-based: UFMC (UF-OFDM)

Universal Filtered MultiCarrier (UFMC) has recently been proposed by Alcatel-Lucent Bell Laboratories [VWS+13], and it is also referred to UF-OFDM in the literature [WSC14]. UFMC

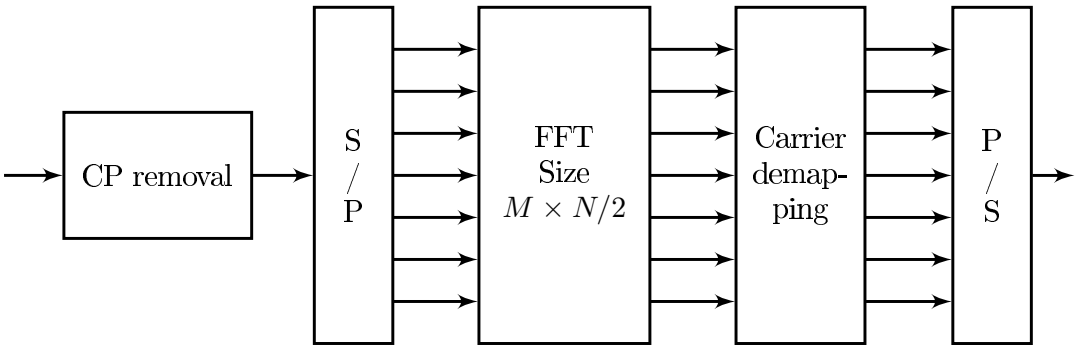

Figure 2-5: BF-OFDM receiver scheme.

is a combination of ZP-OFDM (traditional CP-OFDM where the CP is replaced by a Zero Padding (ZP)) and filtered-OFDM: each OFDM symbol at the output of the IDFT is filtered and the ZP is used to absorb the filter transient response. In the absence of a multipath channel, UFMC holds the orthogonality of the subcarriers. Nevertheless, the orthogonality is no longer sustained as the time spreading of the channel increases and only soft protection against multipath effects is possible at the receiver. At the reception, the multiuser interferences coming from time and frequency asynchronism are first reduced by applying a window on the received UFMC block symbols [SW14]. This windowing is similar to the one used for WOLA-OFDM. It has to be noted that this processing destroys the subcarrier orthogonality even if the channel is perfect. Finally a FFT of size two times greater than the IFFT used at the transmission is applied to the received UFMC block symbols and only even subcarrier indexes are kept. It is important to note that the complexity of the receiver can be reduced by collecting additional samples corresponding to the length of the ZP and using an overlap-and-add method to obtain the circular convolution property [MWG+02]. In this case, the required FFT size is identical to the size of the IFFT used at the transmission. All existing and already developed OFDM-based designs are applicable to UFMC such as MIMO, channel estimation/equalization, pilot, synchronization, PAPR reduction (DFT precoding or any others approaches).

The filter is predefined and set to reduce the out of band radiation of a single resource block composed of 12 subcarriers. Any bandpass filter that covers the subcarriers of the user of interest may be used. The Dolph-Chebyshev filter has been initially proposed [VWS+13] because it provides a good trade-off between filter length and out of band reduction. However other choices are also possible [WWS15, WWSdS14], for instance methods to design filters that provide improved robustness to carrier frequency offset (CFO) and timing offset (TO) also have been reported.

2.2 WF with real orthogonality: FBMC-OQAM

Despite the large success of CP-OFDM as the multicarrier benchmark, it has to deal with the many requirements envisaged in future generation physical layer. Indeed, the capability of using non-contiguous spectrum with a relaxed synchronization are the main challenges of the desired future waveform that OFDM cannot fulfill. In fact, the poor localized frequency response of rectangular transmit filter of CP-OFDM induces high level of Out-Of-Band (OOB) radiation. Besides, the rectangular receive filter also brings an important amount of interference from other asynchronous users [FBM16]. In order to overcome the main OFDM shortcomings, Filter-Bank based MultiCarrier (FBMC) systems have been proposed as an alternative to

OFDM offering better frequency localization and flexible access to the available resources.

The key-idea of FBMC is to use well-frequency localized prototype filters (like PHYDYAS [VIS+09] and IOTA [LFAB95]), instead of the OFDM rectangular one, providing thus better adjacent channel leakage performance compared to OFDM. In order to ensure orthogonality between adjacent symbols and adjacent subcarriers, while keeping maximum spectral efficiency, Nyquist constraints on the prototype filter combined with Offset Quadrature Amplitude Modulation (OQAM) are used. In OQAM, the in-phase and the quadrature components of a given QAM symbol are time staggered by half a symbol period, $N/2$ (i.e. $T/2$). The duration of the prototype filters is usually a multiple of the FFT size ($L = KN$), where K is called the overlapping factor.

Using OQAM modulation, the real-valued input symbols are phase-shifted by multiples of $\pi/2$ along both time and frequency axis. The pre-processed data is then filtered in the frequency domain (i.e. Frequency spread filtering). Actually, since FBMC prototype filters are usually designed by applying the frequency sampling technique, the number of non-zero samples in the frequency response is given by $P = 2K - 1$ i.e. the number of multicarrier symbols which overlap in the time domain [Bel12c].

2.3 WF without orthogonality: FBMC-QAM

As previously discussed, filter-bank based waveforms use a per-subcarrier filtering, reducing thus out-of-band emission and providing more flexibility to meet the future physical layer requirements. As emphasized earlier, such enhancements are at the price of orthogonality condition that only holds in the real domain and is no longer valid in the presence of practical channels. Indeed, the self-interference inherent to OQAM-based schemes can be as strong as the useful signal power [BLRR+10], [ZLRM12]. This is a major problem when considering spatial multiplexing with maximum likelihood detection [ZR14]. In fact, the proposed iterative interference cancellation schemes are limited by error propagation induced by the residual interference signal. In order to overcome this problem, it has been demonstrated, in [AS97] and [VBRB06], that the interference power must be small and should be kept under a certain threshold, in order to counteract the error propagation phenomenon and consequently make more efficient the interference cancellation scheme. In order to achieve this objective and reduce the interference level, the authors in [ZLRM12] were the first to propose the utilization of QAM modulation, instead of OQAM one, in FBMC systems. Actually, a significant part of self-interference is avoided by only transmitting QAM symbols every signalling period $nT, n \in \mathbb{Z}$. In other words, the interference induced by OQAM symbols transmitted in $(2n+1)\frac{T}{2}, n \in \mathbb{Z}$ is no longer considered [ZR14]. Such a combination is called FBMC-QAM systems. In order to improve the performance of FBMC-QAM symbols, new prototype filters have been designed, optimizing simultaneously spectrum localization, self-interference level, and overall spectral efficiency [YKK+15].

3. MIMO Technologies

3.1 Overview

3.1.1 Presentation and interests

A multi-input multi-output (MIMO) system [PGNB04] is a system which uses several antennas at both transmission and reception, contrary to a single-input single-output system which uses only one antenna at both sides.

For ideal propagation channel, i.e. for line of sight (LOS) radiocommunications, a MIMO system allows us to focus the transmitted energy in the receiver direction by steering a beam in the latter. In a same manner a beam may also be steered at reception in the transmitter direction. In this case, the MIMO system is a set of two beamformers, generating an improvement of the budget link for a given transmitted power.

For multi-paths propagation channels, a MIMO system allows us to extract the spatial diversity present at both transmission and reception in order:

- to improve the budget link
- to spatially multiplex several statistically independent data streams at the same time on the same bandwidth.

The improvement of the budget link allows to increase the reliability, the range or the date rate of the communication by choosing higher order constellations. The spatial multiplexing allows to increase the data rate without any change in the constellation.

3.1.2 MIMO schemes

Two families of MIMO schemes at transmission, corresponding to closed-loop and open-loop schemes respectively may be implemented.

Closed-loop schemes correspond to schemes using channel state information (CSI) at transmission. In Frequency Division Duplexing (FDD) systems, this CSI is estimated by the receiver and sent to the transmitter through a feedback link. This requires slow variations of the channel and generates some additional "latency" in the processing. For this reason, these schemes are not selected for MTC links.

Open-loop schemes do not use any CSI at transmission. Open-loop schemes which improve the budget link at reception do not implement spatial multiplexing but use spatio-temporal coding (STC) at transmission [TSC98]. The most famous STC, optimized for $N_t = 2$ transmit antennas, is the Alamouti STC [Ala98b]. Among open-loop schemes which use spatial multiplexing we may cite the V-BLAST scheme [Fos96] or STC with spatial multiplexing such as the Golden code [BRV05]. The open-loop schemes are the ones which are considered in this project for MTC links.

3.2 Coupling of MIMO technology with MC waveforms

3.2.1 MIMO for OFDM waveforms

The coupling of the MIMO technology with OFDM waveforms consists in implementing the MIMO schemes on each sub-carrier of the OFDM waveform. This is a straightforward task thanks to the orthogonality of the sub-carriers in the complex domain whatever the selectivity

degree of the propagation channel, provided that the CP size remains greater than or equal to the delay spread of the channel. Indeed, under this assumption, each sub-carrier sees a flat fading channel without any inter-symbol interference (ISI) and any inter-carrier interference (ICI), which allows us to obtain the performance of MIMO links for single carrier waveforms in flat fading channels. For this reason, the MIMO for CP-OFDM will be the reference for WONG5.

3.2.2 MIMO for filtered MC waveforms

On the contrary, the coupling of the MIMO technology with filtered MC-waveforms may be more difficult, depending on the amount of residual ISI and ICI at reception and the scheme considered. Indeed, Spatial Multiplexing with linear receivers applied to filtered MC waveforms give the same performance as CP-OFDM. However, when STC is considered the residual ISI and ICI could break the properties of the coding scheme.

Filtered MC waveforms which are said to be orthogonal in the complex domain (WOLA-OFDM, UFMC, N-Continuous OFDM, FMT) are in fact orthogonal only for propagation channels which are not too frequency selective. For such channels and for such MC waveforms, the use of MIMO technology is straightforward. However, it will be interesting to evaluate in the project the degree of frequency selectivity over which the performance of the MIMO schemes for these MC-waveforms degrade.

However, filtered MC waveforms which are not orthogonal in the complex domain (FBMC-OQAM, Laped-OFDM-OQAM, WCP-COQAM, FBMC-QAM, GFDM) generate both ISI and ICI at reception. These interference explain the strong performance degradation of most of the standard MIMO schemes used for CP-OFDM, even for propagation channels which are relatively weakly frequency selective . For this reason, new MIMO schemes, aiming at mitigating the effects of ISI and ICI, are required for non orthogonal filtered MC waveforms.

4. MIMO for filtered waveforms

4.1 WF with complex orthogonality or near complex orthogonality

As aforementioned, this study focuses on open-loop systems. Two schemes will be assessed for the considered waveforms: Alamouti and V-Blast.

4.1.1 Alamouti

☐ Description

The Alamouti scheme aims at enhancing the reliability of the link by exploiting the channel diversity. Indeed, transmitting multiple copies of the signal over different channel realizations improves the probability to properly recover the information. At the receiver side, the different copies are linearly combined.

For this study, we will consider a 2×1 system based on the following code :

$$\begin{array}{c} \text{time slots} \longrightarrow \\ \text{transmit antennas} \downarrow \; \frac{1}{\sqrt{2}} \begin{pmatrix} s_1 & s_2 \\ s_2^* & -s_1^* \end{pmatrix} \end{array} \tag{4.1}$$

The transmitted signal can therefore be expressed as follows:

$$\mathbf{s} = \mathbf{s_0} + \mathbf{s_1} + \mathbf{n} \tag{4.2}$$

with $\mathbf{n}$ the Additive White Gaussian Noise realization over two time slots (assuming a dependant and identical distribution) and

$$\begin{cases} \mathbf{s_0} = \frac{1}{\sqrt{2}}[s_1 H_{0,T_1} \quad s_2 H_{0,T_2}] & \text{for Antenna 0} \\ \mathbf{s_1} = \frac{1}{\sqrt{2}}[s_2^* H_{1,T_1} \quad -s_1^* H_{1,T_2}] & \text{for Antenna 1} \end{cases} \tag{4.3}$$

By applying a ZF detection, the estimated symbols $\tilde{\mathbf{s}}$ can be determined as shown below :

$$\tilde{s_1} = \frac{\sqrt{2}\left(s(T_1)H_{0,T_1}^* + \left((s(T_2)H_{1,T_2}^*\right)^*\right)}{|H_{0,T_1}|^2 + |H_{1,T_2}|^2} \tag{4.4}$$

$$\tilde{s_2} = \frac{\sqrt{2}\left(\left(s(T_1)H_{1,T_1}^*\right)^* + s(T_2)H_{0,T_2}^*\right)}{|H_{1,T_1}|^2 + |H_{0,T_2}|^2} \tag{4.5}$$

☐ Scenario Description

The parameters described in Table 4-1 are considered for performance assessment. OFDM and UFMC waveforms are compared in the broadband LTE configuration (10MHz).

The tap-delay table of the BRAN-E channel model is reminded in Table 4-2.

☐ Simulation Results

The first simulation aims at assessing the performance gain provided by the Alamouti scheme over the corresponding single antenna system. The results are depicted in Figure 4-1.

Table 4-1: Simulation parameters

Simulation parameters	
Channel Model	Bran-E
Type	Rician fadings
Speed	5, 50, 100 km.h^{-1} @ 5.5GHz
Constellations	QPSK, 16-QAM, 64-QAM
Decoding	ZF Hard
Channel Estimation	1-tap every symbol periods
Channel Realizations	100
OFDM parameters	
FFT size	1024
CP length	72
Number of Resource blocks	50
Number of active subcarriers	$50 \times 12 = 600$
Sampling Frequency F_e	15.36 MHz (15kHz subcarrier spacing)
RB bandwidth	180 kHz
UFMC parameters	
FFT size, F_e, subcarrier spacing	same as OFDM
Filter	Dolph-Chebyshev, 73 taps, 40dB rejection

Table 4-2: Bran-E tap-delay

delay [ns]	0	10	20	40	70	100	140	190	240	320	430	560	710	880	1070	1280	1510	1760
Average Power [dB]	-4.9	-5.1	-5.2	-0.8	-1.3	-1.9	-0.3	-1.2	-2.1	0	-1.9	-2.8	-5.4	-7.3	-0.6	-13.4	-17.4	-20.9

We can observe that for small constellations (QPSK), the Alamouti scheme provided a significant SNR gain for all the considered speeds: about 5dB SNR gain for a Raw BER$=10^{-2}$ for all the speeds. It can be explained by the extra diversity provided by the multiplexing. Indeed the channels are rather uncorrelated : measured correlation of 0.05 for 5 km.h^{-1}, 0.20 for 50 km.h^{-1} and 0.14 for 100 km.h^{-1}. However, for larger constellations (64-QAM), the performance of the Alamouti scheme is degraded and the MIMO scheme proves to be even worse than the SISO configuration for 100 km.h $^{-1}$. It can be explained by the partial channel compensation and the fact that the coherence time of the channel becomes too short for the Alamouti to perform well. as weel as the hypothesis we did for the receiver.

The second simulation aims at comparing the considered waveforms for the different speeds and constellations. The simulation results are depicted in Figure 4-2. We can observe that OFDM and UFMC exhibit the same performance. It is an expected result as they have identical symbol duration and thus equivalent robustness against Doppler impairments.

In the following, we will provide additional results with the new waveforms proposed in the context of Wong5 project, namely BF-OFDM and FFT-FBMC.

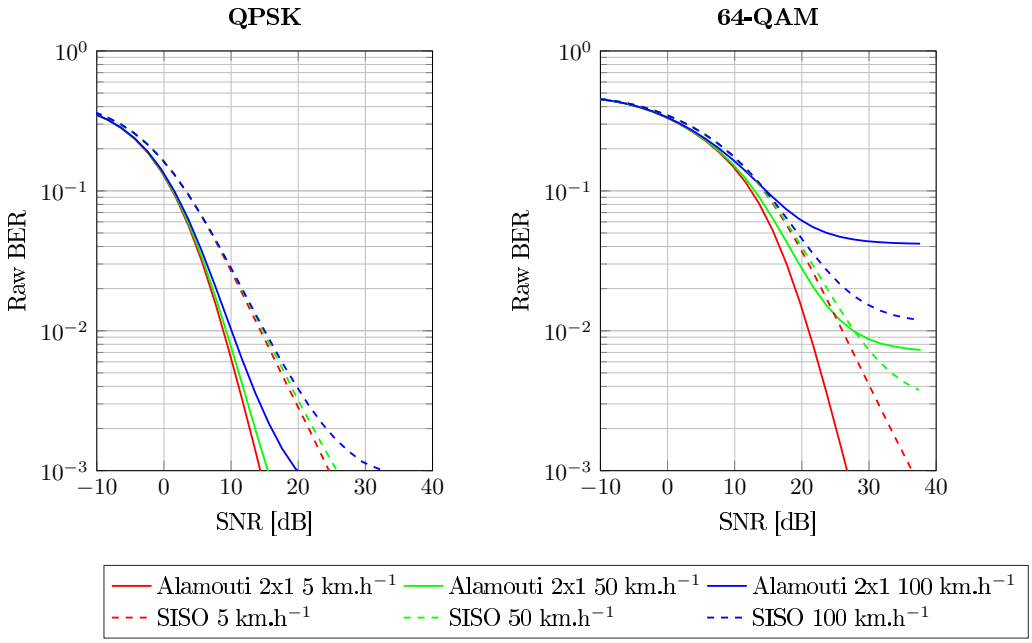

Figure 4-1: Performance Gain provided by the Alamouti scheme with respect to the single antenna configuration

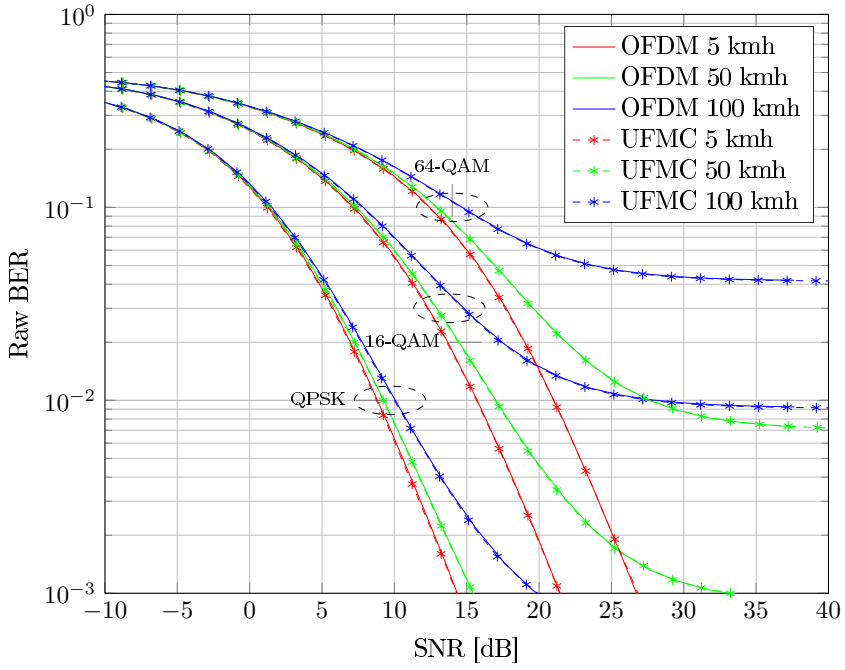

Figure 4-2: Performance obtained by the considered waveforms with Alamouti scheme

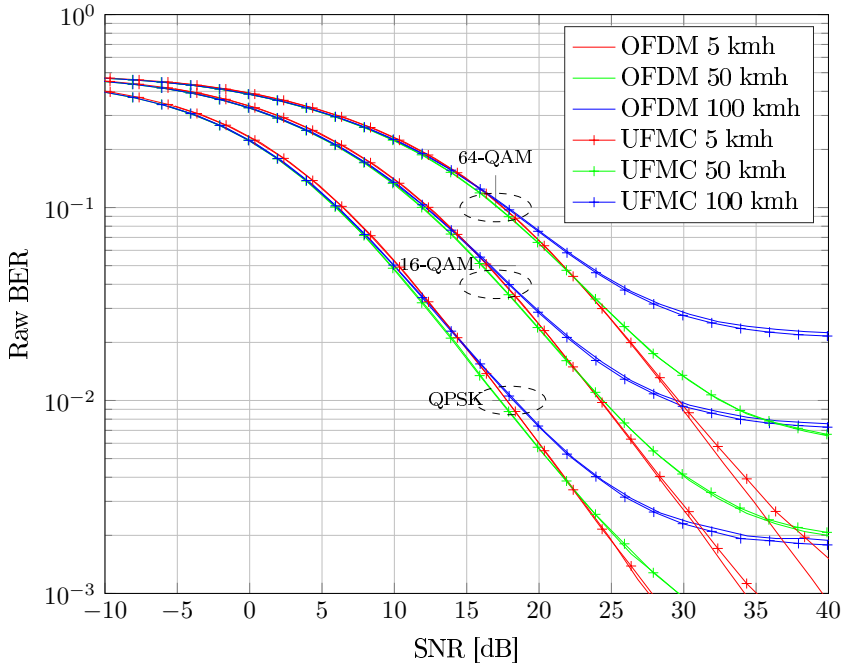

Figure 4-3: Performance obtained by the considered waveforms with V-BLAST scheme

4.1.2 Spatial-Multiplexing V-Blast

☐ Description

The second multiple antennas scheme which is addressed in this study is the Spatial-Multiplexing V-BLAST. This scheme aims at improving the throughput by transmitting independent data stream over the available transmit antennas. To be able to properly recover the information the number of receive antennas N_r must be higher or equal to the number of transmit antennas N_t.

The simulation parameters is the same as for the Alamouti section and is given Figure 4-1.

☐ Simulation Results

For the study, a system 2×2 is considered with a Zero-Forcing based detection. The comparison between the considered waveforms is depicted in Figure 4-3. Like with the Alamouti scheme, we can observe that OFDM and UFMC exhibit the same performance.

In the following, we will provide additional results with the new waveforms proposed in the context of Wong5 project, namely BF-OFDM and FFT-FBMC.

4.2 WF with real orthogonality: state of the art

This section revisits the techniques that have been specifically designed for MIMO-FBMC/OQAM systems. First, the emphasis is put on schemes that achieve spatial multiplexing gains assuming non-high frequency selective channels. Next, it is pursued the development of MIMO techniques that achieve spatial diversity.

4.2.1 Spatial multiplexing schemes

In MIMO spatial multiplexing, we consider N_T antennas are used to transmit N_T data symbols and N_R antennas are used to collect the transmitted signals. The vector of the demodulated signals over all the receive antennas at a given frequency-time position (q, k), after phase compensation is expressed in matrix formulation as

$$\mathbf{r}_q[k] = \mathbf{H}_q \Bigg(\mathbf{d}_q[k] + \underbrace{\sum_{(m,\tau)\in\Omega_{q,k}} \mathbf{d}_m[k-\tau]\Gamma_{qm}[\tau]}_{j\mathbf{u}_q[k]} \Bigg) + \check{\mathbf{w}}_q[k], \tag{4.6}$$

where $\mathbf{H}_q$ denote the $(N_R \times N_T)$ channel matrix, $\mathbf{d}_q[k]$ the symbol vector, $\Gamma_{qm}[\tau]$ is the tansmultiplexer response coefficient with τ is the time delay index, and $\check{\mathbf{w}}_q[k] = \theta_q^*[k]\mathbf{w}_q[k]$. Equivalently, (4.6) can be compactly expressed as

$$\mathbf{r}_q[k] = \mathbf{H}_q(\mathbf{d}_q[k] + j\mathbf{u}_q[k]) + \check{\mathbf{w}}_q[k], \tag{4.7}$$

Linear equalization as ZF and MMSE in FBMC/OQAM context can be performed as described in [TJH07] where a virtually transmitted vector $\mathbf{c}_q[k] = \mathbf{d}_q[k] + j\mathbf{u}_q[k]$ is considered instead of the effective one. The vector $\mathbf{r}_q[k]$ represents the input of the equalizer having as output the equalized virtually transmitted vector $\tilde{\mathbf{c}}_q[k]$:

$$\tilde{\mathbf{c}}_q[k] = \mathbf{G}_q^H \mathbf{r}_q[k], \tag{4.8}$$

where $\mathbf{G}_q \in \mathbb{C}^{N_R \times S}$ is the equalization matrix based on the ZF or MMSE criterion, namely

$$\mathbf{G}_q^{MMSE} = (\mathbf{H}_q\mathbf{H}_q^H + \sigma\mathbf{I})^{-1}\mathbf{H}_q^H \tag{4.9}$$

$$\mathbf{G}_q^{ZF} = (\mathbf{H}_q\mathbf{H}_q^H)^{-1}\mathbf{H}_q^H. \tag{4.10}$$

Then, the real part retrieval of $\tilde{\mathbf{c}}_q[k]$ yields the real equalized data vector $\tilde{\mathbf{d}}_q[k]$ [TJH07], i.e.

$$\tilde{\mathbf{d}}_q[k] = \Re(\tilde{\mathbf{c}}_q[k]) \tag{4.11}$$

The intrinsic interference in FBMC/OQAM can be seen as a 2D-ISI in the time-frequency plane since it depends on the transmitted data symbols in the neighborhood around the considered position (q, k). Therefore, the Maximum Likelihood (ML) detection should perform a 2D-Viterbi algorithm. However, due to the huge complexity of the optimal detection algorithms, it is very difficult to implement them in the context of MIMO-FBMC/OQAM. Consequently in order to achieve close to the optimal ML detection, different suboptimal solutions have been proposed in the literature. Most of these solutions are based on interference estimation and cancellation.

4.2.1.1 MMSE-ML and Rec-ML receivers

The first attempt to estimate the intrinsic interference and then perform cancellation has been proposed in [ZLRB10] where the interference is estimated using a linear MIMO equalizer. The proposed receiver is called MMSE-ML scheme and is depicted in Fig. 4-4. As we have seen, the MMSE equalizer provides an estimation of the virtual transmitted symbol vector $\mathbf{c}_q[k] = \mathbf{d}_q[k] + j\mathbf{u}_q[k]$. Therefore, an evaluation of the interference terms is available by taking only the imaginary part of $\tilde{\mathbf{c}}_q[k]$. This estimation is used to cancel the interference

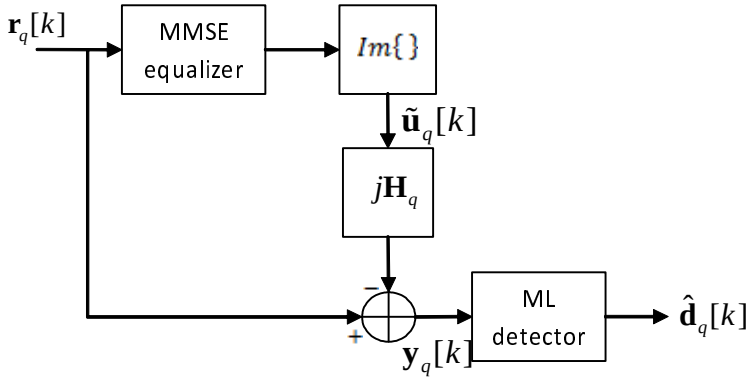

Figure 4-4: Basic scheme of the MMSE-ML receiver

contribution from the received vector $\mathbf{r}_q[k]$. Hence, the obtained vector $\mathbf{y}_q[k]$ is expressed as [ZLRB10]:

$$\begin{aligned}\mathbf{y}_q[k] &= \mathbf{r}_q[k] - j\mathbf{H}_q\tilde{\mathbf{u}}_q[k] \\ &= \mathbf{H}_q(\mathbf{d}_q[k] + j\boldsymbol{\epsilon}_q[k]) + \check{\mathbf{w}}_q[k],\end{aligned} \tag{4.12}$$

where $\tilde{\mathbf{u}}_q[k]$ is the estimated interference vector given by $\tilde{\mathbf{u}}_q[k] = \mathfrak{Im}\{\tilde{\mathbf{c}}_q[k]\}$, and $\boldsymbol{\epsilon}_q[k] = \mathbf{u}_q[k] - \tilde{\mathbf{u}}_q[k]$ is the interference estimation error.

Assuming perfect interference estimation, that is $\boldsymbol{\epsilon}_q[k] \approx \mathbf{0}$, we consider that the vector $\mathbf{y}_q[k]$ at the output of the interference canceller is free of interference. Thus, ignoring the presence of $\boldsymbol{\epsilon}_q[k]$ term, we perform a conventional ML detector. One of the advantages of this receiver is the fact that it does not introduce any processing delay in the system; the interference is estimated from the current received vector and is immediately removed. However, this receiver is based on the assumption that $\mathbf{y}_q[k]$ is free of interference. But unfortunately, the error term in equation (4.12) is obviously non-zero ($\boldsymbol{\epsilon}_q[k] \neq 0$). Consequently, it is clear that we cannot reach the optimal bit-error-rate performance as if there is no interference.

In order to improve the performance, the outputs of the MMSE-ML detector can be exploited and used as tentative decisions to estimate again the interference as shown in Fig. 4-5. This receiver is referred to as Rec-ML (Recursive ML). The advantage of this receiver is that the tentative decisions are now more reliable.

When the transmitter structure is based on space-time bit interleaved coded modulation, it is possible to implement an iterative receiver based on the turbo principle. The first stage is a space-time equalizer, which mitigates the interference and provides soft information to the second stage, where a classical soft-input soft-output binary decoder is employed [ZLR11a] as shown in Fig. 4-6.

At the transmitter side, the binary information enters a convolutional encoder to produce an encoded binary sequence which is bit-interleaved by a random interleaver. Then, the interleaved bits are mapped by a memoryless modulator into symbols belonging to a PAM constellation set $\mathbb{A}$ with cardinality of $2^{\frac{q}{2}}$, where $\frac{q}{2}$ is the bit number in the PAM symbol. After that, the PAM symbols are demultiplexed onto N_T branches (corresponding to N_T antennas). Over each branch the data are sent to the FBMC/OQAM modulator and then transmitted through the radio channel. At the receiver side, the signal in each receive antenna branch is demodulated, forming thus demodulated N_R-vectors $\mathbf{r}_q[k]$.

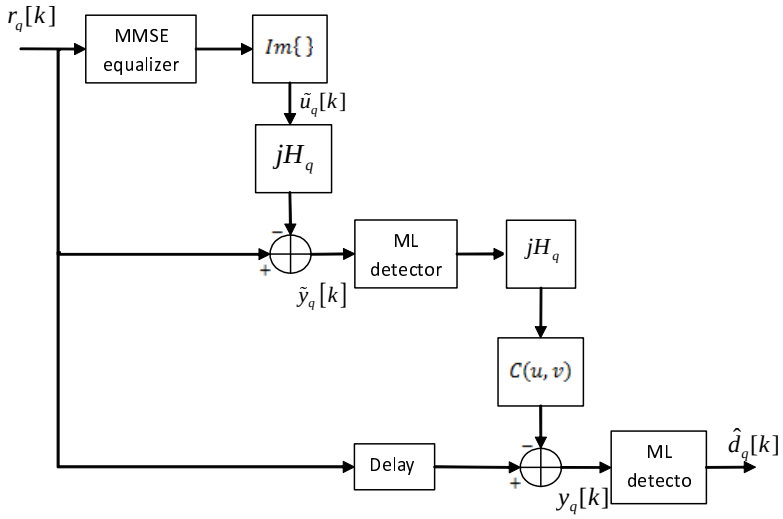

Figure 4-5: structure of the Rec-ML receiver

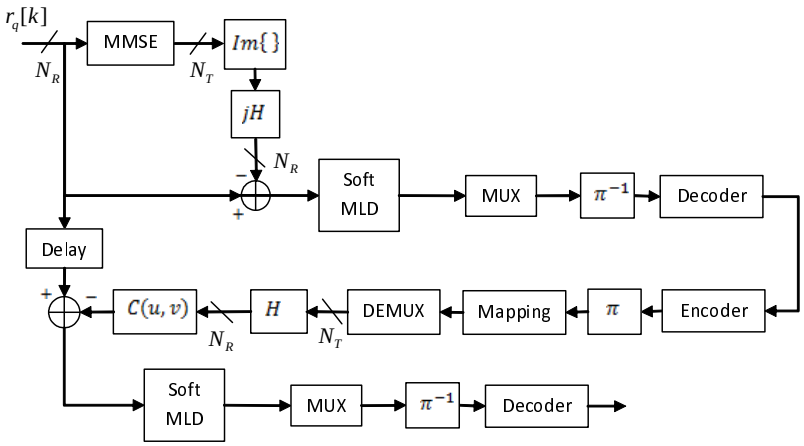

Figure 4-6: coded FBMC scheme

The soft ML detectors (Soft MLD in Fig. 4-6) provide soft outputs in the form of LLR (Log-likelihood ratio) values [SLW03,HtB03]. Then, these soft values are multiplexed, deinterleaved, and decoded to provide decision bits. Thus, the interference estimation is improved since the information bits are encoded and some errors would be corrected.

4.2.1.2 Partial interference cancellation

While in the previous section, the first MMSE equalizer was used to directly estimate the overall intrinsic interference, in this section, the receiver is composed of a tentative detector stage followed by a partial interference estimator as shown in Fig. 4-7.

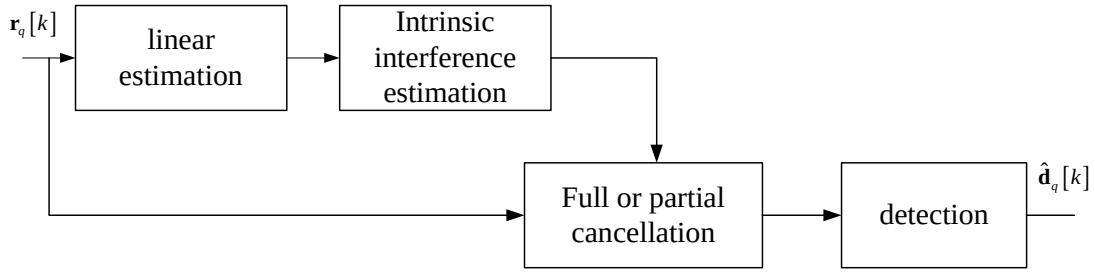

Figure 4-7: General receiver structure

In [ZLR11b] the partial interference cancellation (PaIC) with Viterbi detection receiver has been proposed where the optimum performance is almost reached but the complexity is significantly reduced. ISI cancellation is effective only under some strict conditions. One of these conditions is that the ISI must be sufficiently small. Unfortunately, the intrinsic interference, in FBMC, has the same power as the desired symbol. Hence, a receiver composed of a tentative detector giving decisions which serve to partially cancel the interference, followed by a Viterbi detector matching the non-canceled ISI has been proposed.

In this scheme the set $\Omega_{q,k}$ is split into subsets $\Omega'_{q,k}$ and $\Omega''_{q,k}$. Equation (4.6) becomes

$$\begin{aligned}\mathbf{r}_q[k] &= \mathbf{H}_q\Bigg(\mathbf{d}_q[k] + \sum_{(m,\tau)\in\Omega'_{q,0}} \mathbf{d}_m[k-\tau]\Gamma_{qm}[\tau] \\ &\qquad + \sum_{(m,\tau)\in\Omega''_{q,0}} \mathbf{d}_m[k-\tau]\Gamma_{qm}[\tau]\Bigg) + \check{\mathbf{w}}_q[k] \\ &= \mathbf{H}_q\Big(\mathbf{d}_q[k] + j\mathbf{u}'_q[k] + j\mathbf{u}''_q[k]\Big) + \check{\mathbf{w}}_q[k] \end{aligned} \tag{4.13}$$

The interferences $j\mathbf{u}'_q[k]$ and $j\mathbf{u}''_q[k]$ are respectively the interferences associated to the subsets $\Omega'_{q,k}$ and $\Omega''_{q,k}$. The first stage of the receiver producing tentative decisions and an interference cancellation performed only over the set $\Omega''_{q,k}$

Assuming that the intrinsic interference resulting from the set $\Omega''_{q,k}$ has been completely removed, and that consequently interference only comes from the remaining set $\Omega'_{q,k}$, a main Viterbi detector is then performed. Depending on the set $\Omega'_{q,k}$ a 2D-Viterbi detector can be required. However, designing a 2D-Viterbi is quite challenging and therefore, for simplicity reasons, it was chosen to limit the size of the set $\Omega'_{q,k}$ in order to perform a 1D Viterbi detection.

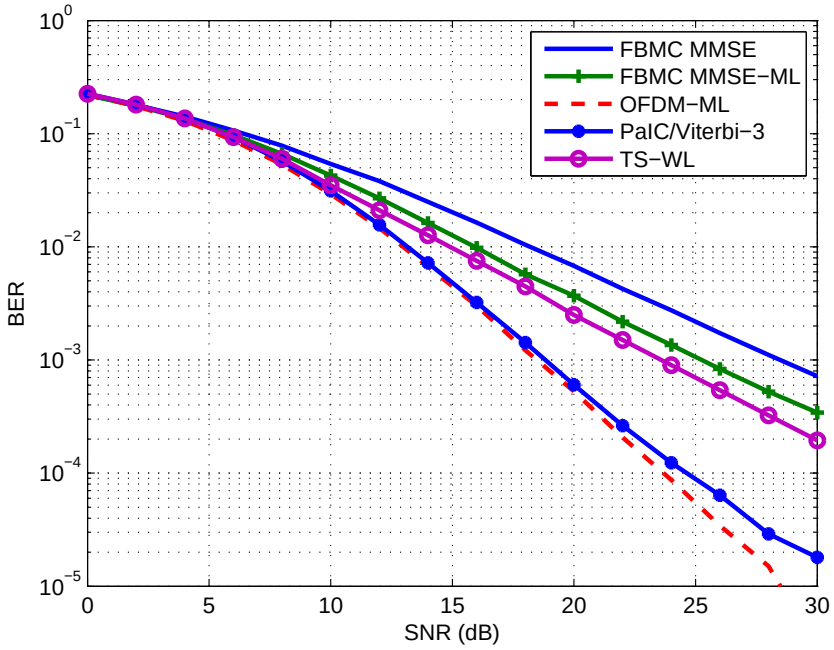

Figure 4-8: BER performance comparison of interference cancellation receiver in 2×2 SM system

In [ZLR16], the authors show that for PHYDYAS filter the set $\Omega'_{q,k}$ which achieve a best tradeoff between complexity and performance is given by:

$$\Omega'_{q,k} = \{(q, k-1); (q, k+1)\} \tag{4.14}$$

The Remaining ISI power in this case is 0.3638 while the total interference is given by

$$\sum_{(q,\tau)\neq(0,0)} |\Gamma_{qm}[\tau]|^2 = 1. \tag{4.15}$$

After removing the interference and assuming perfect interference estimation, the vector $\mathbf{y}_q[k]$ is expressed as

$$\mathbf{y}_q[k] = \mathbf{H}_q(\mathbf{d}_q[k-1]\Gamma_{qq}[-1] + \mathbf{d}_q[k] + \mathbf{d}_q[k+1]\Gamma_{qq}[+1]) + \breve{\mathbf{w}}_q[k]. \tag{4.16}$$

The receiver complexity strongly depends on that of the Viterbi detector. When a spatial multiplexing system with N_T transmit antennas is considered, the Viterbi detector has to compute $M_a^{i\times N_T}$ branch metrics, where M_a is the number of all possible symbols $d_q[k]$ (constellation size) and i is the number of the taps ($i = 3$ for the first set). In order to reduce the receiver complexity, the Viterbi detection algorithm can be replaced by the M-Algorithm [AM84] which keeps only a fixed number (J) of inner states instead of all the inner states $(M_a^{(i-1)\times N_T})$. Hence, the M-algorithm has to compute only $J \times M_a^{N_T}$ branch metrics.

4.2.1.3 Simulation results

In this section we present the simulation based BER performance of the considered receivers. We have tested the receivers in a 2×2 SM system. The number of subcarrier is $M = 1024$, and the data symbols are 4-OQAM modulated. Perfect channel state information at the receiver side is assumed. Fig. 4-8 shows the BER performance of the MMSE, MMSE-ML,

and PaIC/Viterbi receivers. Those receivers are compared to the OFDM-ML. We remark that we obtain better BER performance than the MMSE-ML one; we note an SNR gain of about $1\ dB$ with respect to MMSE-ML. But the performance of IC-ML still remains far from the optimum one. This performance limitation is due to the reliability level of the MMSE equalizer. Furthermore, the MMSE equalizer achieves exactly the same performance than OFDM-MMSE. We also show the simulation results for MMSE-ML and Rec-ML receivers using the (171,133)

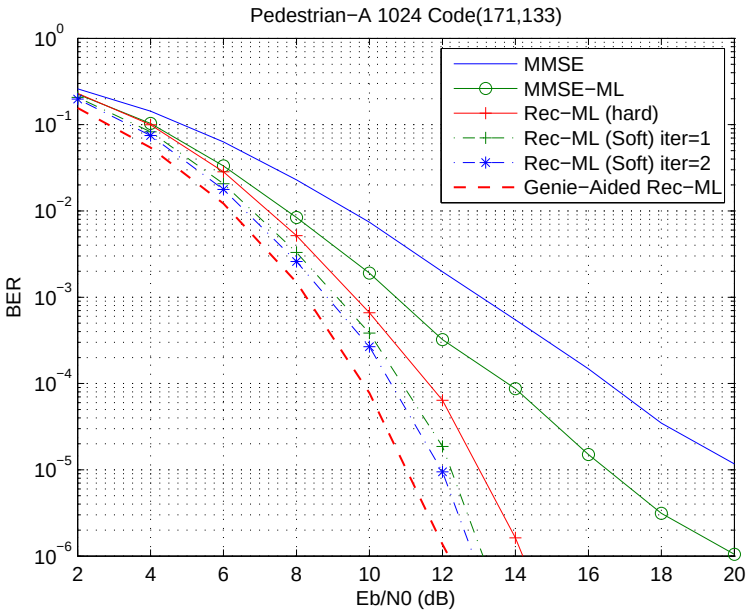

Figure 4-9: BER performance of the FBMC receiver using soft interference cancellation in 2×2 MIMO case and scenario 3

convolutional encoding . In order to improve the interference cancellation, we estimate the interference by using soft decided symbols. The soft received symbols are determined by calculating their expectation values from their Log-Likelihood ratios that calculated using the BCJR algorithm. We test the soft Rec-ML receiver with the same parameters as given previously. Fig. 4-9 depicts the obtained BER performance of the soft Rec-ML receiver. For the sake of comparison, the BER performance of the hard Rec-ML receiver is also depicted. One can observe a performance improvement by using soft interference estimation. However, there is still a performance gap of about $1\ dB$ at $BER = 10^{-4}$ between the Genie-Aided and the soft Rec-ML receiver with 2 iterations. It is worth noting that we do not observe more performance improvement with more than 2 iterations.

4.2.2 Spatial diversity schemes

The application of space time block codes (STBC) or space time treillis codes (STTC) in a straightforward manner to the FBMC/OQAM leads to the appearance of an inherent interference which cannot be easily removed [LSL10]. For example, the difficulty to apply the Alamouti scheme with FBMC can be conceptually explained by the fact that the Alamouti scheme relies on a complex orthogonality whereas FBMC/OQAM has only a real orthogonality that cannot lead to the same type of equations [LSL10]. To tackle this drawback, some works have been carried out on this topic. This section reviews most of these works and summarizes their important results.

4.2.2.1 Transmit diversity schemes

Bellanger proposed a single delay STTC for FBMC/OQAM [Bel08] wherein the same sequence of symbols is transmitted through two transmit antennas ($N_T = 2$) with a delay. This scheme avoids totally the intrinsic interference related to the prototype filter. However, the proposed processing of the received signals leads to a sequence of a weighted sum of data symbols in time domain. Indeed, the received signals after the FBMC demodulation is given by

$$\begin{aligned} r_q[k] =& H_2(q)\left(d_q[k-1] + ju_q[k-1]\right) \\ &+ H_1(q)\left(d_q[k] + ju_q[k]\right) + w_q[k], \end{aligned} \tag{4.17}$$

where $H_1(q)$ and $H_2(q)$ are the channel coefficients at subcarrier q between the receive antenna and both transmit antennas. Then, the following sequence is formed:

$$v_q[k] = \Re\left(H_2(q)^* r_q[k] + H_1(q) r_q[k+1]^*\right) \tag{4.18}$$

which yields :

$$\begin{aligned} v_q[k] =& |H_2(q)|^2 d_q[k-1] + 2\Re\left(H_1(q)H_2(q)^*\right) d_q[k] \\ &+ |H_1(q)|^2 d_q[k+1] + \Re(H_2(q)^* w_q[k]) \\ &+ \Re(H_1(q) w_q[k+1]^*) \end{aligned} \tag{4.19}$$

Thus the data symbols are recovered from the obtained sequence through the maximum likelihood technique, with the help of the Viterbi algorithm. Furthermore, this scheme is quite sensitive to the phase and amplitude of the channels. Indeed, it is shown in [Bel08] that when one of the transmission paths has a much larger magnitude than the other, then the proposed approach exhibits similar performance as single delay STTC. However, it is fairly sensitive to the relative phases of the channel coefficients when their magnitudes are similar, while the single delay STTC scheme is not. The decoding process has been extended to the case of $N_T > 2$ antennas in [LRZ09]. For $N_T = 2$, an iterative decoding method has been proposed to cancel the intrinsic interference and the obtained performance can slightly outperform CP-OFDM.

4.2.2.2 Pseudo Alamouti scheme for CP-FBMC/OQAM

CP-FBMC/OQAM was basically proposed in [LS08] for the SISO case to solve the performance floor problem when using high order constellations with selective channels. CP introduction in this context aims to avoid complexity increase by retaining one-tap equalization but at the expense of spectral efficiency. We present this scheme in this section because it provides a possibility to perform Alamouti coding as it is shown in [LLS09].

The main idea of CP-FBMC/OQAM is that the symbols first pass through an FBMC/OQAM modulator. Then the modulated signal is grouped into successive blocks with size M. Then CP is appended to each block in time domain before transmitting. On the receiver side, after CP removing and applying the FFT a one-tap ZF equalization is carried out. Then the ZF equalized signals are transformed back to time domain by IFFT. Finally the resulting equalized signal is fed to the FBMC/OQAM demodulator. The pseudo Alamouti in [LLS09] is an extension of the CP-FBMC SISO transceiver to 2x1-MISO system with an adaptation of the Alamouti coding/decoding. Indeed, the Alamouti encoder is performed after the FBMC/OQAM modulator in a block-wise manner with the block size of M symbols. In order to keep the Alamouti orthogonality, both symbol blocks transmitted simultaneously at the second period

are reversed. The Alamouti decoding is performed instead of the ZF equalization after the first FFT. The authors in [LLS09] show, by simulations, that due to a specific and efficient channel estimation (CE) method [LJL+07], the proposed pseudo Alamouti transceiver can outperform the Alamouti OFDM scheme. Nevertheless, it is worth noting that the simulation results in [LLS09] are obtained by considering a prototype filter with an overlapping factor of $K = 1$. This avoids any interference between useful data in the time domain.

4.2.2.3 Alamouti coding scheme for CDMA-FBMC

The authors in [LSL10] showed that the 2×1 Alamouti coding can be performed when it is combined with code division multiple access (CDMA). It is shown in [LSLB] that it is possible to have a complex orthogonality with FBMC/OQAM thanks to a subset of CDMA Walsh-Hadamard (WH) codes. That is because when using a subset of $N_c/2$ spreading codes of length N_c the FBMC interference is cancelled during the CDMA despreading operation, which allows us to recover a complex orthogonality property. At the transmitted side, complex symbols are grouped into blocks of $N_c/2$ symbols. Each symbol d_u (with $u = 1, ..., N_c/2$) within a group is spread by a Walsh-Hadamard code c_u of length of N_c. The resulting $N_c/2$ spread signals are summed, which gives us an N_c-block of complex symbols. Then, the N_c-blocks thus formed are fed to the FBMC/OQAM modulator either in frequency-wise or in time-wise.

At the receiver side and after FBMC/OQAM demodulating, the N_c-blocks are formed from the received symbols. Then, each N_c-block is despread by using the $N_c/2$ codes. Assuming that the channel coefficient H is constant along the N_c-block, it is shown that one can obtain at the despreading output:

$$r_u = Hd_u + w_u \tag{4.20}$$

where $u \in \{1, ..., N_c/2\}$, and d_u is a complex data symbol. Therefore, the principle in this proposal is to take advantage of the orthogonality property resulting from the CDMA-FBMC/OQAM combination to obtain a new MIMO Alamouti scheme with FBMC.

Two different approaches with Alamouti coding are proposed [LSL10], by considering either a CDMA spreading in the frequency or in the time domain. If the CDMA spreading is carried out in the frequency domain, the Alamouti decoding scheme can only be applied if the channel is assumed to be flat.

For the 2×1 Alamouti scheme with time spreading CDMA-FBMC/OQAM, two strategies are elaborated for implementing the MIMO space-time coding scheme. Strategy 1 implements the Alamouti over pairs of adjacent frequency domain samples whereas the strategy 2 processes the Alamouti coding scheme over pairs of spreading codes. The authors show that Strategy 2 appears to be more appropriate since it requires less restrictive assumptions on the channel variations across the frequencies. Let $d_{m,1}$ and $d_{m,2}$ denote two complex data symbols to be transmitted at subcarrier "m", and c_1 a c_2 two spreading codes of length N_c. After spreading, antenna 1 transmits the complex symbols

$$a_m^{(1)}[k] = c_1[k]d_{m,1} + c_2[k]d_{m,2}^* \qquad \text{for } k = 1, ..., N_c, \tag{4.21}$$

whereas antenna 2 transmits

$$a_m^{(2)}[k] = c_1[k]d_{m,2} - c_2[k]d_{m,1}^* \qquad \text{for } k = 1, ..., N_c. \tag{4.22}$$

The received symbols at subcarrier q and after the despreading with the codes c_1 and c_2 are respectively:

$$\begin{aligned} r_{q,1} &= H_1(q)d_{q,1} + H_2(q)d_{q,2} + w_{q,1} \\ r_{q,2} &= H_1(q)d^*_{q,2} - H_2(q)d^*_{q,1} + w_{q,2} \end{aligned} \tag{4.23}$$

which can be rewritten in a matrix form as:

$$\begin{bmatrix} r_{q,1} \\ r^*_{q,2} \end{bmatrix} = \begin{bmatrix} H_1(q) & H_2(q) \\ -H_2(q)^* & H_1(q)^* \end{bmatrix} \begin{bmatrix} d_{q,1} \\ d_{q,2} \end{bmatrix} + \begin{bmatrix} w_{q,1} \\ w^*_{q,2} \end{bmatrix} \tag{4.24}$$

Therefore, under some channel hypothesis, the combination of Alamouti with complex CDMA-FBMC/OQAM is possible without increasing the complexity of the Alamouti decoding process. Furthermore, in the case of a frequency selective channel, FBMC/OQAM keeps its intrinsic advantage with a SNR gain in direct relation with the CP length.

4.2.2.4 Block-wise Alamouti scheme for FBMC

Renfors *et al.* in [RIS10] have proposed a solution to combine the Alamouti scheme with FBMC/OQAM, where the Alamouti coding is performed in a block-wise manner inserting gaps (zero-symbols and pilots) in order to isolate the blocks. This solution is feasible when the FBMC/OQAM transmultiplexer impulse response $\Gamma_{qm}[\tau]$ is conjugate symmetric along the time axis. That is, $\Gamma_{qm}[\tau] = \Gamma_{qm}[-\tau]^*$. Let $\{d^1_m[k]\}$ and $\{d^2_m[k]\}$ be two data symbol blocks in the time-frequency domain simultaneously transmitted from antenna 1 and antenna 2, respectively. After that, the time-reversal version of the aforementioned data blocks are transmitted as follows: the first antenna transmits $\{-d^2_m[N-k]\}$ whereas the second one transmits $\{d^1_m[N-k]\}$ [RIS10], where N is the block length. Assuming that the channels H_1 and H_2 are invariant during the transmission of both symbol blocks, the first signal block collected at the receive antenna can be written as:

$$\begin{aligned} y^1_q[k] =& H_1 \sum_m \sum_\tau d^1_m[k-\tau]\Gamma_{qm}[\tau] \\ &+ H_2 \sum_m \sum_\tau d^2_m[k-\tau]\Gamma_{qm}[\tau] + w^1_q[k] \end{aligned} \tag{4.25}$$

where $w^1_q[k]$ is the noise term. The second received signal block is:

$$\begin{aligned} y^2_q[k] =& H_2 \sum_m \sum_\tau d^1_m[\tau-k+N]\Gamma_{qm}[\tau] \\ &- H_1 \sum_m \sum_\tau d^2_m[\tau-k+N]\Gamma_{qm}[\tau] + w^2_q[k] \end{aligned} \tag{4.26}$$

Then, we have:

$$\begin{aligned} y^2_q[N-k]^* = H^*_2 \sum_m \sum_\tau d^1_m[k+\tau]\Gamma_{qm}[\tau]^* \\ - H^*_1 \sum_m \sum_\tau d^2_m[k+\tau]\Gamma_{qm}[\tau]^* + w^2_q[N-k]^* \end{aligned} \tag{4.27}$$

which can be written as:

$$y_q^2[N-k]^* = H_2^* \sum_m \sum_\tau d_m^1[k-\tau]\Gamma_{qm}[\tau] - H_1^* \sum_m \sum_\tau d_m^2[k-\tau]\Gamma_{qm}[\tau] + w_q^2[N-k]^* \quad (4.28)$$

This last expression stands thanks to the fact that $\Gamma_{qm}[\tau]$ is conjugate symmetric along the time axis ($\Gamma_{qm}[\tau] = \Gamma_{qm}[-\tau]^*$). Therefore, applying the Alamouti decoding, we have:

$$\begin{aligned} r_q^1[k] &= \frac{H_1^* y_q^1[k] + H_2 y_q^2[N-k]^*}{|H_1|^2 + |H_2|^2} \\ &= \sum_m \sum_\tau d_m^1[k-\tau]\Gamma_{qm}[\tau] + \frac{H_1^* w_q^1[k] + H_2 w_q^2[N-k]^*}{|H_1|^2 + |H_2|^2}, \end{aligned} \quad (4.29)$$

and

$$\begin{aligned} r_q^2[k] &= \frac{H_2^* y_q^1[k] - H_1 y_q^2[N-k]^*}{|H_1|^2 + |H_2|^2} \\ &= \sum_m \sum_\tau d_m^2[k-\tau]\Gamma_{qm}[\tau] + \frac{H_2^* w_q^1[k] - H_1 w_q^2[N-k]^*}{|H_1|^2 + |H_2|^2}. \end{aligned} \quad (4.30)$$

The terms $\sum_m \sum_\tau d_m^i[k-\tau]\Gamma_{qm}[\tau]$, with $i \in \{1,2\}$, contain the transmitted data symbols $d_q^i[k]$ and also the inherent interference. Since the interference term $\sum_{m\neq q} \sum_{\tau\neq 0} d_m^i[k-\tau]\Gamma_{qm}[\tau]$ is purely imaginary, the transmitted data symbols are easily estimated by a simple real part retrieval.

4.2.2.5 Interference cancellation in Alamouti coding scheme for FBMC

The issue of performing the Alamouti coding in FBMC/OQAM is the presence of the intrinsic interference. To remove this interference term, some works based on iterative interference estimation and cancellation were also carried out. Unfortunately, detection schemes with interference estimation and cancellation are subject to error propagation and are not always effective [ZLR11b]. Therefore, the challenge in this kind of schemes is to mitigate the error propagation through iterations [AS97].

Aiming to reduce the intrinsic interference power, the authors in [ZR13] propose some arrangements in the space-time and frequency block coding (STBC, SFBC) in order to improve the signal to interference ratio (SIR). The idea behind these arrangements is to automatically remove an important part of the interference only by performing the adequate Alamouti decoding. Then, the remaining interference is cancelled iteratively by interference estimation and cancellation procedure. The selected arrangement that minimizes the remaining interference consists of interleaving two Alamouti blocks (in time or in frequency domain) with an alternating rule in position of the minus sign between both blocks. The following matrices

illustrates the selected arrangement:

$$D_1 = \begin{bmatrix} \ddots & \vdots & \vdots & \vdots & \vdots & \vdots & \iddots \\ \dots & d_0[-1] & d_0[0] & d_0[1] & d_0[2] & d_0[3] & \dots \\ \dots & d_2[-1] & d_2[0] & d_2[1] & d_2[2] & d_2[3] & \dots \\ \iddots & \vdots & \vdots & \vdots & \vdots & \vdots & \ddots \end{bmatrix}$$

$$D_2 = \begin{bmatrix} \ddots & \vdots & \vdots & \vdots & \vdots & \vdots & \iddots \\ \dots & d_0[-3] & d_0[2] & -d_0[3] & -d_0[0] & d_0[1] & \dots \\ \dots & d_1[-3] & d_1[2] & -d_1[3] & -d_1[0] & d_1[1] & \dots \\ \dots & d_2[-3] & d_2[2] & -d_2[3] & -d_2[0] & d_2[1] & \dots \\ \iddots & \vdots & \vdots & \vdots & \vdots & \vdots & \ddots \end{bmatrix} \tag{4.31}$$

where D_1 and D_2 are the data blocks transmitted at the first and the second antennas, respectively. The proposed Alamouti schemes applied in FBMC/OQAM are tested and it is shown that the BER performance curves converge to the free-interference performance. The

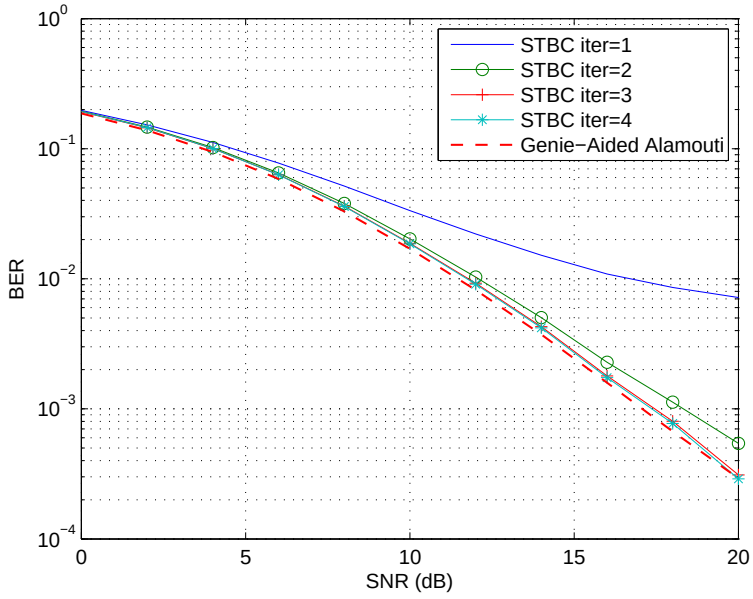

Figure 4-10: Performance of the STBC scheme [ZR13] in FBMC/OQAM using OQPSK modulation

BER performance with OQPSK mapping is shown in Fig. 4-10. The BER performance of the first iteration corresponds to the tentative Alamouti decoding and the BER floor at 7×10^{-3} is due to the remaining interference. However, one can observe that the performance curves reach the Genie-Aided performance after 3 iterations.

It is worth noticing that the weakness of these IIC receivers is the fact that the performance is promptly decayed when higher mapping orders are considered [ZR14, ZR13].

4.2.3 Principal limitations of existing solutions

Because of the intrinsic interference, the full potential performance of FBMC/OQAM cannot be straightforwardly reached when combined with some MIMO schemes. Therefore, specific signal processing techniques had been developed and used. In this section, an overview of known solutions for FBMC/OQAM with Alamouti and SM-ML was presented. Solutions based on iterative interference estimation and cancellation exhibit a significant complexity increase and processing time delays. Moreover, the performance is promptly decayed when higher mapping orders are considered [ZR14, ZR13]. Other solutions have been also presented, which require some modifications in the original FBMC/OQAM structure such as appending a CP in CP-FBMC/OQAM or adding extra FFT/IFFT blocks in FFT-FBMC to restore the complex orthogonality. All the different overviewed solutions for FBMC/OQAM may offer good performance at the expense of either complexity increase or spectral efficiency reduction. Therefore, the combination of FBMC/OQAM modulation with MIMO techniques such as Alamouti coding and SM-ML is still an open issue and a challenging topic. In section 5, we present some perspectives and preliminary new solutions dealing with the association of FBMC/OQAM and MIMO systems.

4.3 WF without orthogonality: state of the art

To reduce the power of the intrinsic interference, it was proposed in [ZLRM12] to modify the conventional FBMC/OQAM system by using Quadrature Amplitude Modulation (QAM) symbols instead of OQAM ones and by transmitting the data symbols on each period T instead of transmitting them on each half period $T/2$. That is, the authors utilize the conventional lattice structure of OFDM with complex-valued symbols and localized filters. Thus, the interference coefficients corresponding to the odd multiples of $T/2$ are avoided, and the overall interference power is reduced. However, as a consequence of this modification, the real orthogonality condition of FBMC/OQAM is no longer satisfied [ZR14]. Therefore, even in SISO system, interference cancellation methods must be applied at the receiver.

4.3.1 Spatial multiplexing

In MIMO spatial multiplexing, the MMSE equalizer is used as the first tentative detector. After interference estimation and cancellation, a conventional ML detection is applied. Fig. 4-11 depicts the obtained BER performance of the FBMC/QAM using PHYDYAS filter. We compare the performance of IIC-ML in FBMC/QAM with the Rec-ML (proposed in [ZLRB10]) one in FBMC/OQAM using -for both of them- the PHYDYAS filter. We also show the BER performance of the OFDM using ML detector. We notice that IIC-ML performance almost converges to the optimum one after 5 iterations. However, one can observe a slight SNR loss less than $0.5\ dB$ compared to the Genie-Aided performance. On the other hand, one can notice that MMSE equalizer for FBMC/QAM exhibits worse BER performance compared to FBMC/OQAM. This is explained by the fact that the intrinsic ISI term in FBMC/QAM is complex as the transmitted data symbols (no orthogonality), whereas in FBMC/OQAM the interference terms are pure imaginary and the data symbols are real-valued (real orthogonality). However, the situation is different with IIC-ML and Rec-ML receivers, we clearly notice that Rec-ML with conventional FBMC/OQAM suffers from the error propagation effect and the BER performance converges to a suboptimal one, whereas the ISI cancellation is effective with IIC-ML in FBMC/QAM system, where we obtain almost the same performance as OFDM-ML.

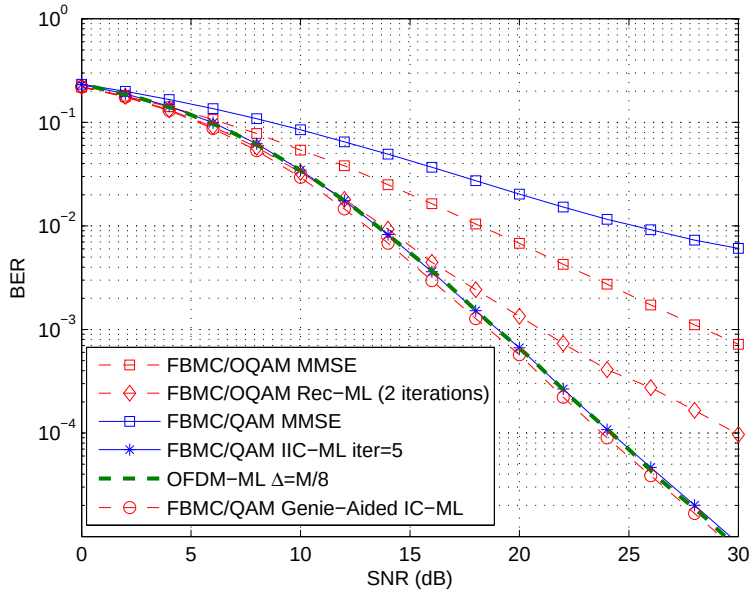

Figure 4-11: Performance of IIC-ML receiver in FBMC/QAM system using PHYDYAS filter and 4-QAM constellation for 2×2 spatial multiplexing

Recently, Sim and *al.* [SKL16] have optimized the prototype filter to reduce the intrinsic interference power in FBMC/QAM. Moreover, they have proposed a layered detection algorithm based on interference cancellation for FBMC-QAM. In this proposed algorithm, the authors have define two thresholds, a selection threshold and a region threshold for efficient interference cancellation. Depending on the value of the subcarrier channel gains, the algorithm decides whether to apply IC or not.

4.3.2 Space-time block coding

As for the STBC decoding, a first Alamouti decoder is used as tentative detector providing tentative estimations of the data symbols. Based on these tentative estimates, the interference canceler calculates an estimation of the interference, and then its contribution is removed from the received vector. After that, the Alamouti decoding is again applied, and the operation is repeated several times. The authors in [ZR14] show by simulations that Alamouti coding scheme with Iterative Interference Cancellation (IIC) applied in FBMC-QAM provides satisfactory performance. Fig. 4-12 depicts the BER performance obtained of the IIC-Alamouti in FBMC-QAM with three iterations and compare them to the OFDM and genie-aided Alamouti performance. This latter is obtained by assuming perfect intrinsic interference cancellation. We observe an SNR loss of only 0.5 dB compared to the genie-aided performance. Nevertheless, the IIC-Alamouti in the FBMC-QAM system exhibits almost the same performance as that obtained with OFDM; this is due to the E_b/N_0 loss caused by the Cyclic Prefix (CP) in OFDM.

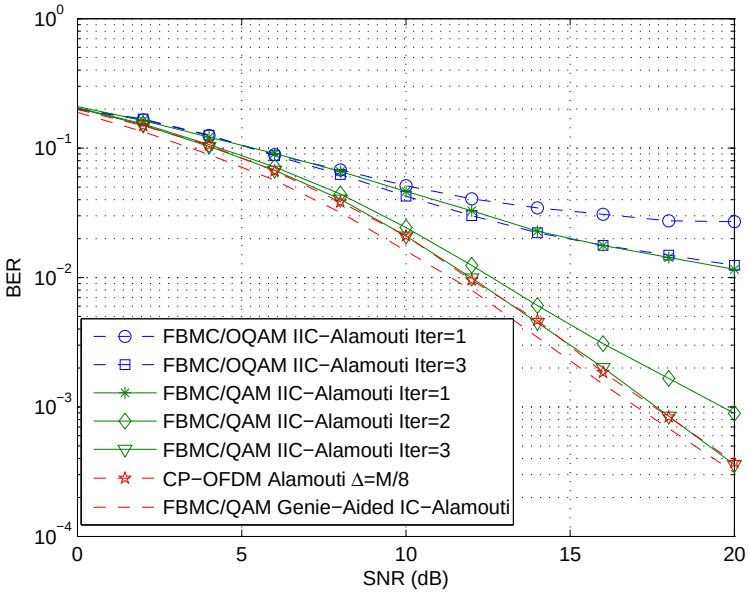

Figure 4-12: Performance of IIC-Alamouti receiver with FBMC-QAM using PHYDYAS filter and 4-QAM constellation.

5. New MIMO tranceiver schemes for filtered waveforms

This section presents preliminary new MIMO transceiver schemes for filtered waveforms which are not orthogonal in the complex domain. Section 5.1 introduces some preliminary ideas about per-carrier joint demodulation-based processing, section 5.2 briefly presents the potential interest of WL processing for FBMC-OQAM waveforms, section 5.3 presents preliminary results about Frequency-Spreading detectors and finally section 5.4 introduces briefly the principle of a multi-carrier approach using linear receivers.

5.1 Carrier per Carrier processing

5.1.1 ML with 3 sub-carriers

5.1.1.1 Reception model

☐ Transmitted Alamouti FBMC-OQAM signals

Let us recall that the baseband signal, $s(t)$, of an OQAM signal transmitting the complex symbols c_k, of duration T_s, can be written as

$$s(t) = \sum_k c_k^r v(t - kT_s) + jc_k^i v(t - kT_s - T_s/2) \tag{5.1}$$

where c_k^r and c_k^i are real quantities corresponding to the real part and the imaginary part of the associated QAM symbol c_k respectively, whereas $v(t)$ is the pulse shaping filter. Defining the real symbols b_{2k} and b_{2k+1} by $b_{2k} \triangleq (-1)^k c_k^r$ and $b_{2k+1} \triangleq (-1)^k c_k^i$ respectively, it is straightforward to show that $s(t)$ can also be written as

$$s(t) = \sum_k j^k b_k v(t - kT) \triangleq \sum_k a_k v(t - kT) \tag{5.2}$$

where $T \triangleq T_s/2$ and $a_k \triangleq j^k b_k$. Equation (5.2) means that the OQAM signal (5.1) can also be interpreted as a signal which transmits, without any staggering operation, the complex symbols a_k, or the real symbols b_k, with a symbol duration equal to T. We consider a radio communication system that employs the Alamouti scheme, with two transmit antennas [Ala98b], on each sub-carrier of a FBMC-OQAM waveform, as depicted at Fig. 5-1. Under this assumption and using (5.2), the baseband signals, $s_1(t)$ and $s_2(t)$, transmitted by antennas 1 and 2 respectively, can be written as

$$s_1(t) = \sum_{l=0}^{L-1} \sum_k \left[a_{l,2k-1} v(t-(2k-1)T) - a_{l,2k}^* v(t-2kT) \right] j^l e^{j\pi \frac{lt}{T}} \tag{5.3}$$

$$s_2(t) = \sum_{l=0}^{L-1} \sum_k \left[a_{l,2k} v(t-(2k-1)T) + a_{l,2k-1}^* v(t-2kT) \right] j^l e^{j\pi \frac{lt}{T}} \tag{5.4}$$

Here, $(.)^*$ means complex conjugate, L is the number of sub-carriers, $1/2T = 1/T_s$ is the sub-carrier spacing, $v(t)$ is the prototype filter and $a_{l,k} \triangleq j^k b_{l,k}$, where $b_{l,k}$ is the real symbol transmitted (without the Alamouti encoding) at time kT on sub-carrier l. Note that the Alamouti scheme is applied here to the complex symbols

$$a_{l,k} = j^k b_{l,k} \tag{5.5}$$

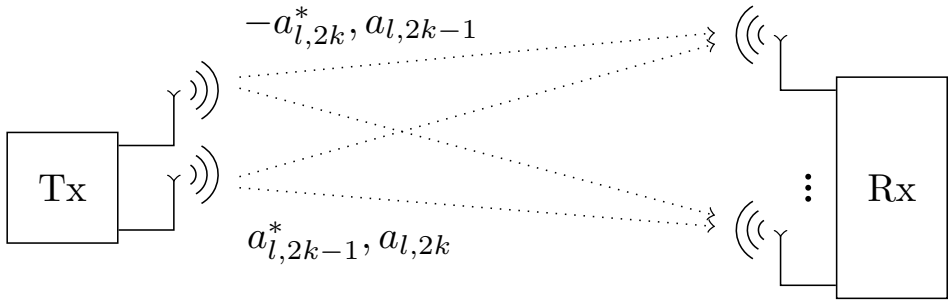

Figure 5-1: MIMO $2 \times N$ system using Alamouti space-time coding per sub-carrier

(which are either real or purely imaginary) of duration $T = T_s/2$, and not to the associated QAM symbols,

$$c_{l,k} \triangleq (-1)^k [b_{l,2k} + j b_{l,2k+1}] \tag{5.6}$$

of duration T_s, before staggering. This allows to consider spatio-temporal Alamouti code words of duration T_s instead of $2T_s$ and this imposes constant propagation channels over T_s instead of $2T_s$. Note that the Alamouti scheme has already been applied with success to real-valued symbols instead of complex ones in [PCa11].

☐ Received Alamouti FBMC-OQAM signals

Assuming a reception with N antennas, and denoting by $\mathbf{h}_i(t)$ $(i = 1, 2)$ the impulse response vector of the propagation channel between the transmit antenna i and the reception array, the observation vector at time t at the output of the receive antennas is given by

$$\mathbf{x}(t) = \sum_{i=1}^{2} s_i(t) * \mathbf{h}_i(t) + \mathbf{n}(t) \tag{5.7}$$

Here, $*$ is the convolution operation, $\mathbf{n}(t)$ is the background noise vector assumed to be zero-mean, Gaussian, circular, stationary, spatially and temporally white.

☐ Observation model after low-pass filtering

Considering that l_0 is the sub-carrier of interest for the processing we consider, the vector $\mathbf{x}(t)$ is first frequency shifted by $e^{-j\pi l_0 t/T}$ to put the sub-carrier l_0 at baseband. Then an arbitrary low-pass filter, $p(t)$, is applied to the shifted observation vector to isolate the baseband contribution of the sub-carrier l_0 and to remove both the noise outside its bandwidth and the sub-carriers which do not overlap with l_0. The bandwidth B of the filter $p(t)$ must be that of a sub-carrier, i.e. $B = 2/T_s = 1/T$. An example of filter $p(t)$ may be $v^*(-t)$, the matched filter associated with $v(t)$, but this is not mandatory. Under these assumptions, we deduce from (5.7) that the observation vector after frequency shifting and low-pass filtering takes the

form

$$\begin{aligned}\mathbf{x}_p(t) &\triangleq p(t) * \left[e^{-j\pi\frac{l_0 t}{T}}\mathbf{x}(t)\right] \\ &= \sum_{i=1}^{2} p(t) * \left[e^{-j\pi\frac{l_0 t}{T}} s_i(t) * \mathbf{h}_i(t)\right] + \mathbf{n}_p(t) \\ &\triangleq \sum_{i=1}^{2} \mathbf{s}_{ph,i}(t) + \mathbf{n}_p(t) \end{aligned} \tag{5.8}$$

Here, $\mathbf{n}_p(t) \triangleq p(t) * [e^{-j\pi l_0 t/T}\mathbf{n}(t)]$ and $\mathbf{s}_{ph,i}(t) \triangleq p(t) * [e^{-j\pi l_0 t/T} s_i(t) * \mathbf{h}_i(t)]$.

5.1.1.2 Maximum Likelihood receiver

☐ Presentation of the ML approach

The receiver which is proposed in this paper consists first in jointly demodulating, from a ML approach, the sub-carrier of interest, l_0, and the sub-carriers which overlap with the latter after the low-pass filtering operation. Then, the idea is to retain only the demodulated symbols belonging to the sub-carrier of interest, l_0, and to discard the others. The operation of joint demodulation of the overlapped sub-carriers aims at mitigating the ICI for the sub-carrier l_0 instead of considering ICI as an additional noise for l_0. The sub-carriers corresponding to the ICI for the sub-carrier l_0 are then discarded since they will be much better demodulated when they will correspond themselves to the sub-carrier of interest.

In order to take easily into account the potential temporal coloration property of $\mathbf{n}_p(t)$ and to remove the potential influence of the sampling rate, we adopt a continuous time ML approach to develop the proposed receiver. In this context, under the assumptions of section 5.1.1.1, we deduce from (5.8) that the ML joint detection of the symbols belonging to the sub-carrier of interest l_0 and to the $2M$ sub-carriers which overlap with the latter, consists in generating the symbol set $\mathbf{b} = \{b_{l,k}, l_0 - M \leq l \leq l_0 + M, k \in Z\}$ which minimizes the following criterion [MSC12, Ung74][1]

$$\mathrm{C}(\mathbf{b}) = \int_B \left[\mathbf{x}_p(f) - \sum_{i=1}^{2} \mathbf{s}_{ph,i}(f)\right]^H \mathbf{R}_{n,p}^{-1}(f) \left[\mathbf{x}_p(f) - \sum_{i=1}^{2} \mathbf{s}_{ph,i}(f)\right] df; \tag{5.9}$$

where $(.)^H$ means transpose and conjugate whereas $\mathbf{R}_{n,p}(f)$ is the power spectral density matrix of $\mathbf{n}_p(t)$, defined by

$$\mathbf{R}_{n,p}(f) = N_0 \left|p(f)\right|^2 \mathbf{I} \tag{5.10}$$

where N_0 is the power spectral density of $\mathbf{n}(t)$ and $\mathbf{I}$ is the identity matrix. We assume in the following that the propagation channels are known and approximately flat over the bandwidth B. This holds in practice as long as the delay spread of the channels remains much lower than T, which is always true beyond a sufficient number of sub-carriers. Under this assumption, we deduce from (5.8) that $\mathbf{s}_{ph,i}(f)$ can be written as

$$\mathbf{s}_{ph,i}(f) = p(f) s_i\left(f + \frac{l_0}{2T}\right)\mathbf{h}_i = p(f) s_{R,i}\left(f + \frac{l_0}{2T}\right)\mathbf{h}_i \tag{5.11}$$

[1] All Fourier transforms of vectors $\mathbf{x}$ and matrices $\mathbf{X}$ use the same notation where t is simply replaced by f.

where $\mathbf{h}_i \triangleq \mathbf{h}_i(f+l_0/2T) = \mathbf{h}_i(l_0/2T)$ and $s_{R,i}(f+l_0/2T) \triangleq s_i(f+l_0/2T)R_B(f)$, $(i=1,2)$, such that

$$R_B(f) = 1 \text{ for } |f| \leq B/2 \text{ and } R_B(f) = 0 \text{ otherwise} \tag{5.12}$$

Moreover, we assume that $M = 1$, i.e. that only the two adjacent sub-carriers, $l_0 - 1$ and $l_0 + 1$, overlap with the sub-carrier l_0. Note that this assumption is in particular true for the PHYDYAS prototype filter [BLRR+10, Bel10] which is chosen for this work. Besides, to simplify the notations, we denote by $b_{m,k}$ the real-valued symbol $b_{l_0+m,k}$ $(-1 \leq m \leq 1)$ and we consider that $a_{m,k} \triangleq j^k b_{m,k}$. Under these assumptions, we deduce from (5.3) and (5.4) that

$$s_{R,1}\left(f + \frac{l_0}{2T}\right) = R_B(f) \sum_{m=-1}^{1} \sum_{k} \left[a_{m,2k-1} e^{j2\pi Tf}(-1)^m - a^*_{m,2k}\right] e^{-j4\pi kTf} v\left(f - \frac{m}{2T}\right) j^{l_0+m} \tag{5.13}$$

$$s_{R,2}\left(f + \frac{l_0}{2T}\right) = R_B(f) \sum_{m=-1}^{1} \sum_{k} \left[a_{m,2k} e^{j2\pi Tf}(-1)^m + a^*_{m,2k-1}\right] e^{-j4\pi kTf} v\left(f - \frac{m}{2T}\right) j^{l_0+m} \tag{5.14}$$

Using (5.10) and (5.11) into (5.9), we obtain an alternative expression of (5.9) given by

$$\mathrm{C}(\mathbf{b}) = \frac{1}{N_0} \int \left\| \mathbf{x}_R(f) - \sum_{i=1}^{2} s_{R,i}\left(f + \frac{l_0}{2T}\right) \mathbf{h}_i \right\|^2 df \tag{5.15}$$

where

$$\mathbf{x}_R(f) \triangleq R_B(f)\mathbf{x}(f + l_0/2T) \tag{5.16}$$

Criterion (5.15) shows that the joint ML receiver depends on the prototype filter $v(t)$ but does not depend on the form of the low-pass filter $p(t)$, provided that $p(f) \neq 0$ for $-B/2 \leq f \leq B/2$. Inserting (5.13) and (5.14) into (5.15), we obtain after straightforward manipulations

$$\mathrm{C}(\mathbf{b}) = \frac{1}{N_0} \int \left\| \mathbf{x}_R(f) - R_B(f) \sum_{m=-1}^{1} \sum_{k} e^{-j4\pi kTf} v\left(f - \frac{m}{2T}\right) j^{l_0+m}(-1)^k \mathbf{h}_{m,k}(f) \right\|^2 df \tag{5.17}$$

where

$$\mathbf{h}_{m,k}(f) = j b_{m,2k-1}\left[e^{j2\pi Tf}(-1)^{m+1}\mathbf{h}_1 + \mathbf{h}_2\right] + b_{m,2k}\left[e^{j2\pi Tf}(-1)^m \mathbf{h}_2 - \mathbf{h}_1\right] \tag{5.18}$$

□ Alternative expression of $\mathrm{C}(\mathbf{b})$

To express the criterion $\mathrm{C}(\mathbf{b})$ as a function of discrete-time signals only, we must introduce a set of quantities defined hereafter. We introduce the following quantities: $v_m(t) \triangleq v(t)e^{j\pi mt/T}$, $\mathbf{x}_{Rv,m}(t) \triangleq e^{-j\pi l_0 t/T}\mathbf{x}(t) * R_B(t) * v^*_m(-t)$, $r_m(t) \triangleq v^*(-t) * v_m(t)$ and $r_{R,m,n}(t) \triangleq v^*_n(-t) * R_B(t) * v_m(t)$, for $(-1 \leq m, n \leq 1)$, where we recall that $R_B(t)$ is the inverse Fourier transform of $R_B(f)$. The quantities $\mathbf{x}_{Rv,m}(t)$ and $r_{R,m,n}(t)$ are the inverse Fourier Transform of their Fourier Transform and we then obtain

$$\mathbf{x}_{Rv,m}(t) = \int e^{j2\pi ft}\mathbf{x}_R(f) v^*\left(f - \frac{m}{2T}\right) df \tag{5.19}$$

m \ k	-4	-3	-2	-1	0	1	2	3	4
-1	0.0054	j0.0429	-0.1250	-j0.2058	0.2393	j0.2058	-0.1250	-j0.0429	0.0054
0	0	-0.0668	0	0.5644	1	0.5644	0	-0.0668	0
1	0.0054	-j0.0429	-0.1250	j0.2058	0.2393	-j0.2058	-0.1250	j0.0429	0.0054

Table 5-1: ISI/ICI table of the PHYDYAS prototype filter ($r_m(kT)$) with m Carrier index and k Symbol index

$$r_{R,m,n}(t) = \int e^{j2\pi ft} R_B(f) v^*\Big(f - \frac{n}{2T}\Big) v\Big(f - \frac{m}{2T}\Big) df \tag{5.20}$$

Note that the samples $r_m(kT)$ for $(-1 \leq m \leq 1,\ -4 \leq k \leq 4)$ define the joint ISI/ICI table of the PHYDYAS prototype filter, corresponding to Table 5-1. These samples are zero for $|k| > 4$. The samples $r_{R,m,n}(kT)$ define another ISI/ICI table related to Table 5-1 by the following relations:

$$\begin{cases} r_{R,m,0}\,(kT) = r_m\,(kT) \\ r_{R,0,n}\,(kT) = (-1)^{kn} r_{-n}(kT) \end{cases} \quad \text{for } (-1 \leq m, n \leq 1) \tag{5.21}$$

$$r_{R,1,-1}\,(kT) = r_{R,-1,1}\,(kT) = 0 \tag{5.22}$$

$$r_{R,1,1}\,(kT) = (-1)^k I_1\,(kT) \text{ and } r_{R,-1,-1}\,(kT) = (-1)^k I_{-1}\,(kT) \tag{5.23}$$

where $I_1(kT)$ and $I_{-1}(kT)$ are defined by

$$I_1(kT) = \int_{-\frac{1}{2T}}^{0} e^{j2\pi kTf} \left|v(f)\right|^2 df \tag{5.24}$$

$$I_{-1}(kT) = \int_{0}^{\frac{1}{2T}} e^{j2\pi kTf} \left|v(f)\right|^2 df \tag{5.25}$$

It is easy to verify that $\Re[I_1(kT)] = \Re[I_{-1}(kT)] = r_0(kT)/2$ while $\Im[I_1(kT)] = -\Im[I_{-1}(kT)]$ has an infinite support whose first values are illustrated at Fig. 5-2.

We define the (3×1) and (6×1) vectors $\mathbf{b}_k$ and $\widetilde{\mathbf{b}}_k$ by $\mathbf{b}_k \triangleq [b_{-1,k}, b_{0,k}, b_{1,k}]^T$ and $\widetilde{\mathbf{b}}_k \triangleq [\mathbf{b}_{2k-1}^T, \mathbf{b}_{2k}^T]^T$ and the $(3N \times 1)$ and $(6N \times 1)$ vectors $\widetilde{\mathbf{x}}_{Rv}(kT)$ and $\widetilde{\mathbf{x}}(kT)$ by $\widetilde{\mathbf{x}}_{Rv}(kT) \triangleq [\mathbf{x}_{Rv,-1}^T(kT), \mathbf{x}_{Rv,0}^T(kT), \mathbf{x}_{Rv,1}^T(kT)]^T$ and $\widetilde{\mathbf{x}}(kT) \triangleq [\widetilde{\mathbf{x}}_{Rv}^T((2k-1)T), \widetilde{\mathbf{x}}_{Rv}^T(2kT)]^T$. We also define the $(6 \times 6N)$ channel matrix H by

$$H \triangleq \begin{pmatrix} H_{11} & H_{12} \\ H_{21} & H_{22} \end{pmatrix} \tag{5.26}$$

where the $(3 \times 3N)$ matrices H_{ij} $(1 \leq i, j \leq 2)$ are defined by $H_{11} \triangleq \Lambda_{11} K_1^H$, $H_{12} \triangleq \Lambda_{11}^* K_2^H$, $H_{21} \triangleq -j\Lambda_{11} K_2^H$, $H_{22} \triangleq -j\Lambda_{11}^* K_1^H$, where the (3×3) matrix Λ_{11} is defined by $\Lambda_{11} \triangleq$

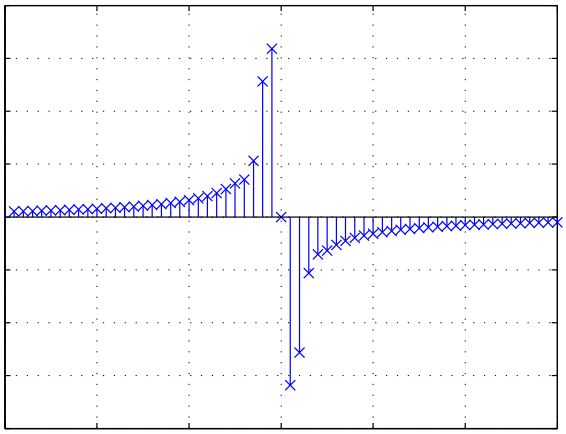

Figure 5-2: $\Im[I_1(kT)]$ as a function of k

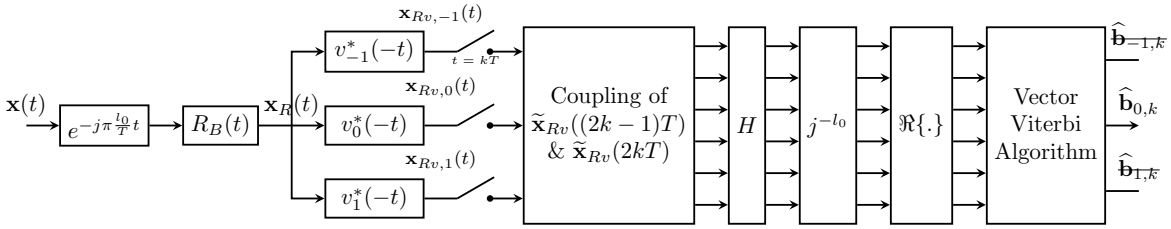

Figure 5-3: Structure of the ML receiver for l_0

$\mathrm{Diag}(1, j, -1)$ whereas the $(3 \times 3N)$ matrix K_i^H $(1 \leq i \leq 2)$ is defined by

$$K_i^H \triangleq \begin{pmatrix} \mathbf{h}_i^H & & \\ & \mathbf{h}_i^H & \\ & & \mathbf{h}_i^H \end{pmatrix} \tag{5.27}$$

Finally, we define the (6×6) matrix $F(k)$ by

$$F(k) \triangleq \begin{pmatrix} F_{11}(k) & F_{12}(k) \\ F_{21}(k) & F_{22}(k) \end{pmatrix} \tag{5.28}$$

where $F_{ij}(k)$ $(1 \leq i, j \leq 2)$ are (3×3) matrices whose coefficients $F_{ij}(k)[2+m, 2+n]$ for

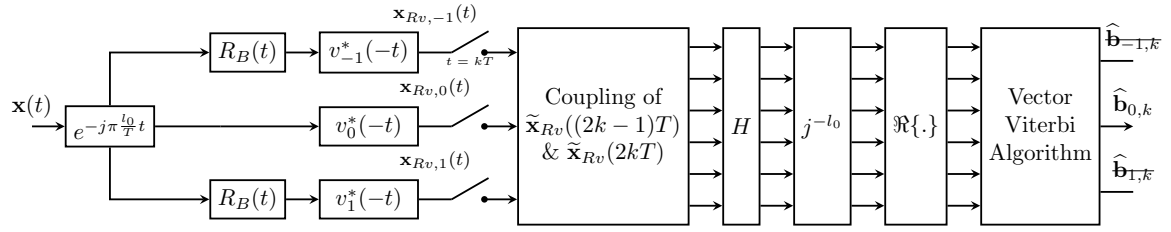

Figure 5-4: Alternative structure of the ML receiver for l_0

$(-1 \leq m, n \leq 1)$ are such that

$$F_{11}(k)[2+m, 2+n] \triangleq j^{n-m}\Bigg\{ \begin{array}{l} \Big[(-1)^{m+n}\mathbf{h}_1^H\mathbf{h}_1 + \mathbf{h}_2^H\mathbf{h}_2\Big] r_{R,n,m}(2kT) \\ +(-1)^{m+1}\mathbf{h}_1^H\mathbf{h}_2 r_{R,n,m}\left((2k-1)T\right) \\ +(-1)^{n+1}\mathbf{h}_2^H\mathbf{h}_1 r_{R,n,m}\left((2k+1)T\right)\Bigg\} \end{array} \tag{5.29}$$

$$F_{12}(k)[2+m, 2+n] \triangleq -j^{n-m+1}\Bigg\{ \begin{array}{l} \Big[(-1)^{m+n+1}\mathbf{h}_1^H\mathbf{h}_2 - \mathbf{h}_2^H\mathbf{h}_1\Big] r_{R,n,m}(2kT) \\ +(-1)^{m}\mathbf{h}_1^H\mathbf{h}_1 r_{R,n,m}\left((2k-1)T\right) \\ +(-1)^{n}\mathbf{h}_2^H\mathbf{h}_2 r_{R,n,m}\left((2k+1)T\right)\Bigg\} \end{array} \tag{5.30}$$

$$F_{21}(k)[2+m, 2+n] \triangleq j^{n-m+1}\Bigg\{ \begin{array}{l} \Big[(-1)^{m+n+1}\mathbf{h}_2^H\mathbf{h}_1 - \mathbf{h}_1^H\mathbf{h}_2\Big] r_{R,n,m}(2kT) \\ +(-1)^{m}\mathbf{h}_2^H\mathbf{h}_2 r_{R,n,m}\left((2k-1)T\right) \\ +(-1)^{n}\mathbf{h}_1^H\mathbf{h}_1 r_{R,n,m}\left((2k+1)T\right)\Bigg\} \end{array} \tag{5.31}$$

$$F_{22}(k)[2+m, 2+n] \triangleq j^{n-m}\Bigg\{ \begin{array}{l} \Big[(-1)^{m+n}\mathbf{h}_2^H\mathbf{h}_2 + \mathbf{h}_1^H\mathbf{h}_1\Big] r_{R,n,m}(2kT) \\ +(-1)^{m+1}\mathbf{h}_2^H\mathbf{h}_1 r_{R,n,m}\left((2k-1)T\right) \\ +(-1)^{n+1}\mathbf{h}_1^H\mathbf{h}_2 r_{R,n,m}\left((2k+1)T\right)\Bigg\} \end{array} \tag{5.32}$$

Using these notations and inserting (5.19) and (5.20) into (5.17), we obtain an alternative expression of $\mathrm{C}(\mathbf{b})$, given by

$$\mathrm{C}(\mathbf{b}) = \frac{1}{N_0}\Bigg\{ -2\sum_k (-1)^k \widetilde{\mathbf{b}}_k^T \Re\Big[j^{-l_0} H\widetilde{\mathbf{x}}(kT)\Big] + \sum_k \sum_i (-1)^{k+i} \widetilde{\mathbf{b}}_k^T F(k-i)\widetilde{\mathbf{b}}_i \Bigg\} \tag{5.33}$$

Using (5.28) and the definition of $\widetilde{\mathbf{b}}_k$, (5.33) can also be written as

$$\mathrm{C}(\mathbf{b}) = \tfrac{1}{N_0}\Bigg\{ \begin{array}{l} -2\sum_k (-1)^k \widetilde{\mathbf{b}}_k^T \Re\Big[j^{-l_0} H\widetilde{\mathbf{x}}(kT)\Big] \\ +\sum_k \sum_i (-1)^{k+i} \Bigg\{ \begin{array}{l} \mathbf{b}_{2k-1}^T F_{11}(k-i)\mathbf{b}_{2i-1} + \mathbf{b}_{2k}^T F_{22}(k-i)\mathbf{b}_{2i} \\ +\mathbf{b}_{2k-1}^T \Big[F_{12}(k-i) + F_{21}^T(i-k)\Big]\mathbf{b}_{2i}\Bigg\}\Bigg\} \end{array} \end{array} \tag{5.34}$$

Using (5.24), (5.25), Table 5-1 and (5.29) to (5.32), it is possible to verify that the (3×3) coupling matrix, $K_{12}[k] \triangleq F_{12}(k) + F_{21}^T(-k)$, between the symbol vectors at odd and even sample times is not zero. More precisely, it can be verified that $K_{12}(k)$ has only two non-zero elements corresponding to $K_{12}(k)[1,1]$ and $K_{12}(k)[3,3]$, which are associated with the

couples $(m,n)=(-1,-1)$ and $(m,n)=(1,1)$ respectively. We deduce from this result that the two sets of symbol vectors $\{\mathbf{b}_{2k-1}\}$ and $\{\mathbf{b}_{2k}\}$ cannot be demodulated separately but have to be jointly demodulated. The problem is then to find the set of symbol vectors, $\widetilde{\mathbf{b}}_k$, which minimizes (5.33).

☐ Interpretation

The vector $\widetilde{\mathbf{x}}(kT)$ appearing in (5.33) contains the samples, at odd and even sample times, $(2k-1)T$ and $2kT$, of the vectors $\mathbf{x}_{Rv,m}(t)$ for $(-1\leq m\leq 1)$. Moreover, expression (5.19) shows that $\mathbf{x}_{Rv,m}(kT)$ is the sample, at time kT, of the output of the matched filter, $v_m^*(-t)$, whose input is $\mathbf{x}_R(t)\triangleq R_B(t)*(e^{-j\pi l_0 t/T}\mathbf{x}(t))$. The structure of the ML receiver for the sub-carrier of interest l_0 is depicted at Fig. 5-3. It is composed of a frequency shifting operation which puts the sub-carrier l_0 at baseband, a low-pass filtering by the ideal filter $R_B(t)$, which keeps the sub-carrier l_0, removes the sub-carriers which do not overlap with l_0 and keeps a temporally white noise inside its bandwidth, a set of three filters, $v_m^*(-t)$ $(-1\leq m\leq 1)$, adapted to the pulse shaping filter of each of the three sub-carriers we jointly demodulate, a sampling operation at the symbol rate T, a coupling of the samples of the matched filters outputs at odd and even time samples, a matched filtering operation to the propagation channels, a derotation operation of the sub-carrier l_0, a real part capture, a decision box implementing the vector Viterbi algorithm and a box which keeps only the decided symbols of the sub-carrier of interest. Using the fact that $R_B(t)*v_0^*(-t)=R_B(t)*v^*(-t)=v^*(-t)$, an equivalent structure of the ML receiver is presented at Figure 5-4, where the filter $R_B(t)$ has been removed from the branch associated with the sub-carrier $m=0$.

☐ Implementation issues and perspectives

Once the propagation channels vectors, $\mathbf{h}_i$ $(i=1,2)$, have been estimated, the first difficulty which is encountered to implement the previous ML receiver is related to the fact that $R_B(t)$ is a non-causal infinite impulse response, impossible to implement. The second difficulty, which is related to the first one, concerns the size of the ISI before decision, which controls the complexity of the vector Viterbi algorithm and which is infinite, as shown by Fig. 5-2, due to the presence of the ideal low-pass filter $R_B(t)$.

In practice, the first difficulty may be solved by replacing in Fig. 5-3 or Fig. 5-4, the filter $R_B(t)$ by an arbitrary low-pass filter $p(t)$, having a bandwidth B, and whose time support is as small as possible to minimize the size of the ISI before decision. One solution may be to choose $p(t)=v^*(-t)$, the filter matched to the PHYDYAS prototype filter. Once this choice has been done, the structures of Fig. 5-3 or Fig. 5-4 may be modified accordingly, by replacing in all parts of these structures, the parameters which are built from the filter $R_B(t)$ by parameters built from $p(t)$. Note that while the structures of Fig. 5-3 and Fig. 5-4 are equivalent for $p(t)=R_B(t)$, they lose their equivalence for $p(t)\neq R_B(t)$. Another approach, alternative to the two previous ones, is to implement, after the low-pass filtering operation by $p(t)$, the joint ML receiver of the three sub-carriers $m=-1,0,1$ under a false assumption of temporally white noise. This is equivalent to consider the optimization criterion (5.9), assuming that $\mathbf{R}_{n,p}(f)=N_0\mathbf{I}$. This approach is justified by the fact that the presence of the filter $R_B(t)$ in the ML structure is directly linked to the noise whitening operation contained in the ML criterion (5.9). For each of the three sub-optimal receivers previously described, the size of the ISI may be strongly reduced with respect to the one of the ML receiver. Despite this fact, one may still decide to constraint the ISI size used in the Viterbi algorithm, or

equivalently the number of states, to have a given size. This will solve the second difficulty and a compromise between performance and complexity must be found. Another option to solve the second difficulty is based on the fact that only two elements of matrix $K_{12}[k]$ are non-zero. This option consists in forcing the decoupling of the metric and to implement two separate receivers for the demodulation of the symbol vectors associated with the odd and even samples time. All these options may be mixed to find the best compromise between performance and complexity. This comparative study of the three sub-optimal receivers jointly with the optimization of the compromise between performance and complexity are out of the scope of this paper and will be analyzed elsewhere.

5.1.2 Alternative ML

As said previously, for both FBMC-QAM and FBMC-OQAM, the intrinsic interference can be seen as a 2D-ISI in the time-frequency domain. Consequently, the complexity of the exact ML estimation is intractable due to the number of states of the can be seen as a. Since the input output relation in both cases can be described using a factor graph representation [KFL01], it is possible to apply message passing algorithm over this graph in order to estimate the posterior probabilities. In this project, we will study and evaluate different suboptimal ML algorithms based on message passing algorithm on factor graphs.

5.1.3 Joint SIC and MMSE/ZF

In section 4.2, we have introduced different algorithms based on interference cancellation for MIMO-FBMC/OQAM and MIMO-FBMC/QAM such as MMSE-ML and Rec-ML. Recently, Sim and *al.* [SKL16] have proposed a layered detection algorithm based on interference cancellation for FBMC-QAM. In this proposed algorithm, the authors have define two thresholds, a selection threshold and a region threshold for efficient interference cancellation. Depending on the value of the subcarrier channel gains, the algorithm decides whether to apply IC or not.

In [IL09], Ikhlef and Louveaux have considered the MMSE ordered successive interference cancellation (MMSE-OSIC) receiver. To further improve the performance of the OSIC receiver, it is possible to combine it with a two-stage SIC. The main idea behind the two stage OSIC receiver is that, after applying the OSIC algorithm once, subtraction of the contribution of the adjacent subcarriers from the subcarrier of interest becomes possible since a first estimate of all streams on all subcarriers is already available. The decisions used here are coming from the first application of the OSIC algorithm. The contributions of the current subcarrier are removed during the second stage of the OSIC algorithm using the most recent estimates of the symbol streams. This means that the interference coming from adjacent subcarriers is always canceled using the results of the first stage, and the interference coming from the subcarrier of interest is canceled using the OSIC technique in the second stage.

In [SL17], the authors have proposed the so-called two-step MIMO maximum likelihood detection receiver with a two-dimensional ordering algorithm for MIMO-FBMC/QAM.

In this project, we will first extend the proposed solutions given in [SKL16] and [SL17] to the case of FBMC/OQAM where the interference level is higher than for FBMC/QAM. We will also evaluate different classes of linear or low complexity equalizer in order to improve the performance of the MMSE-ML, Rec-ML and PaIC schemes described in section 4.2.

5.2 Widely Linear processing

Widely linear (WL) processing, consisting in processing linearly and independently the observed signals and their complex conjugate, outperform linear processing for second-order non-circular signals such as OQAM signals. For this reason, it is worth of consideration for FBMC-OQAM waveforms. In the following, we will try to evaluate the potential of WL processing for both ISI and ICI mitigation, in comparison to linear processing.

5.3 Frequency-Spreading detectors

5.3.1 Introduction

Fitting the communication systems with multiple antennas is a common solution to improve the throughput and the transmission reliability. Although MIMO techniques are well suited with CP-OFDM, the application to FBMC systems is not straightforward mainly due to the inherent interference. For instance, the Maximum-Likelihood detection (ML) requires an important complexity that can not be practically implemented. Indeed, the inherent interference term generated by the 2-D transmultiplexer response requires a large computation overhead because of the ML full research process even for small constellations [Zak12].

When the carrier spacing widens, the channel variations may become appreciable at the layer band level. Consequently, with a simple 1-tap equalization stage the channel effects may not be properly compensated. Therefore the orthogonality would no longer be satisfied and the performance would considerably decrease. Using precoding at the transmitter side and/or multi-tap equalizers is an efficient way to significantly improve the performance for transmissions over highly frequency-selective channels [CPNK14]. In this work, we consider an open-loop system, without any channel knowledge at the transmitter side. The aim of this section is twofold:

- extend linear detectors to multi-tap equalizer using the FS scheme. Indeed, as the symbols are spread over a set of subcarriers with the FS scheme, a per-layer 1-tap detection can be seen as a multi-tap detection at the carrier level.
- study and implement a modified Alamouti coding procedure compatible with FS-based FBMC-OQAM.

5.3.2 Soft-Decision Linear Receivers for Spatial-Multiplexing FBMC/OQAM with Frequency Spreading receiver

5.3.2.1 System Model

An open-loop spatial multiplexing system (SM-MIMO) based on a Bit Interleaved Coded Modulation scheme (BICM) [CTB97] will be considered. The transmitter is fitted with N_T antennas and the receiver with N_R antennas with $N_T \leq N_R$. At any time instant n, N_T data streams are transmitted over the N_T transmit antennas (or layers). The received data stream vector transmitted at carrier k at time instant n will be denoted as $\mathbf{r}_{k,n}$ (length N_R). The corresponding baseband system model can be expressed as:

$$\mathbf{r}_{k,n} = \mathbf{H}_{k,n}\mathbf{s}_{k,n} + \mathbf{n}_{k,n} \tag{5.35}$$

where the channel matrix $\mathbf{H}_{k,n}$ is a $N_R \times N_T$ channel response at frequency k composed of uncorrelated Rayleigh fading gains, $\mathbf{n}_{k,n}$ is the Additive White Gaussian Noise term with

zero-mean and a variance σ_n^2. The noise realizations are assumed statistically independent and identically distributed. $\mathbf{s}_{k,n}$ is the demodulated signal which exact expression depends on the receiver scheme. The symbols are taken from a 2^N-QAM alphabet. The average energy of the constellation per antenna is normalized to unity. Besides, the antennas are assumed spatially uncorrelated. At the receiver side, we assume a perfect Channel State Information (CSI) and perfect synchronization.

Notations :

In the rest of the section, indexes k denotes the carrier index ($k \in [0, M-1]$) and m the subcarrier index ($m \in [0, KM-1]$) with M the number of carrier and K the overlapping factor of the prototype filter.

5.3.2.2 Recall of FBMC/OQAM

☐ Principles

In the framework of 5G and cognitive radio related projects, there has been a renewed interest for FBMC modulation scheme that was introduced in the mid-60s [Cha66]. FBMC is likely to outperform OFDM in its drawbacks, mainly the bit rate limitation due to the cyclic prefix insertion and the poor frequency localization due to the rectangular filter shape at the price of a slightly increased complexity induced by the filtering stages.

With FBMC modulation scheme, the data at each carrier is shaped by a finite pulse filter. The shape of the filter controls the localization of the modulated pulse both in time and frequency domains. However the Balian Low Theorem [FS98] states that it is not possible to obtain a well-localized filter shape in time and frequency that also satisfies the orthogonality between carriers. The key point of FBMC/OQAM is to relax the orthogonality condition by restricting it to the real field and to be able to use a well-localized prototype filter shape. Thus the transmitted data must be real-valued. The QAM symbols are converted into two Pulse Amplitude Modulation (PAM) symbols (corresponding to the in-phase and quadrature components of the complex symbol) that are transmitted with half symbol duration delay to acheive maximum spectral efficiency.

When it comes to the prototype filter, we consider in this study the PHYDYAS filter that has been introduced in [Bel10]. The frequency shape of the filter is determined by $2K-1$ non-zero coefficients G_k ($G_k \neq 0$ for $k \in [0, 2K-1]$ and 0 otherwise).

With a transmission over a multipath channel, the perfect reconstruction would be lost due to the delay spread as no CP is inserted between adjacent symbols. It is assumed that the channel delay spread is far smaller than the filter impulse response: $L \ll KM$ where L denotes the channel spread. It implies that the filter impulse response fluctuations over a time slot comparable to the channel spread are very limited and can be neglected. In other words, the channel can be considered as flat for each carrier. This is the flat fading approximation at the carrier level.

In the literature, two FBMC receiver schemes are commonly considered: PPN-FBMC [SSL02] [Bel10] and FS-FBMC [Bel12b][DBK15]. With the PPN architecture, the data is filtered in the time domain for both the transmitter and the receiver. The receiver is composed of a PPN which decomposes the received sequence (KM samples) into K sequences of M samples before summing them and a M-points FFT. The block diagram of the receiver is depicted in Fig. 5-5. The FS architecture avoids computation redundancies induced by the PPN by replacing the latter by a FFT and thus makes the receiver implementation more straightforward at the expense of larger FFT size. When the FS architecture is used, the equalization

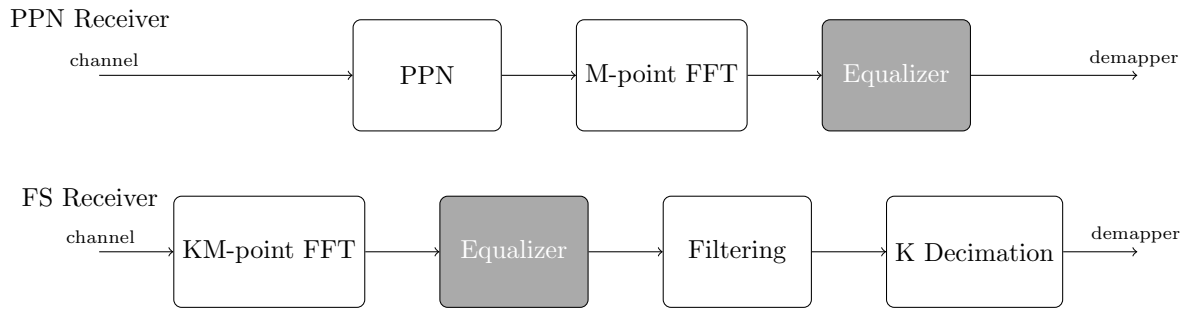

Figure 5-5: PPN and FS receiver schemes

is performed at the ouput of the KM-FFT (at the subcarrier level and not the carrier level as in PPN), and before the filtering stage. The frequency resolution of the FS receiver is thus improved by moving the detection stage before the filtering. This solution proves to be more robust to FFT misalignment and large delay spread channel [Bel12a][DBK15]. The channel estimation must be performed with a spacing frequency of $\frac{1}{KM}$.

☐ PPN Model

The received vector (input of the equalizer) is expressed as follows [Zak12]:

$$\mathbf{r}_{k,n} = \mathbf{H}_{k,n}\left(\mathbf{a}_{k,n} + j\mathbf{u}_{k,n}\right) + \mathbf{n}_{k,n} \tag{5.36}$$

where $\mathbf{a}_{k,n}$ is the transmitted PAM symbol vector ($\sigma_a^2 = 1/2$) and $\mathbf{u}_{k,n}$ the real inherent interference induced by the non-complex orthogonality.

☐ FS Model

The received vector (input of the equalizer) is expressed as follows [DBK15]:

$$\mathbf{r}_{m,n} = \mathbf{H}_{m,n}(\mathbf{b}_{m,n} + \mathbf{i}_{m,n}) + \mathbf{n}_{m,n} \tag{5.37}$$

$$\text{with } \mathbf{b}_{m,n} = \begin{cases} G_{K-1}a_{z,n}e^{j\theta_{z,n}} & \text{if } z \in \mathbb{N} \\ G_{K+l-1}a_{\lfloor z \rfloor,n}e^{j\theta_{\lfloor z \rfloor,n}} + G_{l-1}a_{\lfloor z+1 \rfloor,n}e^{j\theta_{\lfloor z+1 \rfloor,n}} & \text{otherwise} \end{cases} \tag{5.38}$$

where $\lfloor x \rfloor$ is the largest integer less than or equal to x and with $l \equiv m - K + 1 (\mathrm{mod}\ K)$ and $z = \frac{m-K+1}{K}$.

$\mathbf{i}_{m,n}$ is the complex interference term induced by the non-complex orthogonality, and $\theta_{k,n}$ the phase term that ensures a phase shift of $\pi/2$ between adjacent PAM symbols in time and frequency [Zak12].

Assuming an ideal channel and a noiseless transmission, the transmitted PAM symbols $\mathbf{a}_{k,n}$ are recovered by filtering with the prototype filter G and compensating the phase term $e^{j\theta_{k,n}}$ [DBCK14]. Finally, the real part is taken in order to remove the inherent interference which is purely imaginary:

$$\mathbf{a}_{k,n} = \Re\left[e^{-j\theta_{k,n}}\left(\sum_{p=0}^{2K-1} G_p(\mathbf{b}_{kK+p,n} + \mathbf{i}_{kK+p,n})\right)\right] \tag{5.39}$$

The channel is assumed to be time invariant. Therefore to simplify the notations, the instant time index n will be omitted in the rest of the paper for both PPN and FS system models.

5.3.2.3 Soft Linear Detection

This section is dedicated to the detection stage. As stated in introduction, this paper focuses on linear detection with both Zero-Forcing (ZF) and Minimum Mean Square Error (MMSE) equalization criterion adressed.

The equalizer is linear, i.e. the incoming signal $\mathbf{r}_k$ [resp. $\mathbf{r}_m$] is processed with a linear filter $\mathbf{W}_k$ [$\mathbf{W}_m$]. The output of the equalizer $\tilde{\mathbf{r}}_k$ [resp. $\tilde{\mathbf{r}}_m$] can be expressed as:

$$\tilde{\mathbf{r}}_k = \mathbf{W}_k \mathbf{r}_k \tag{5.40}$$

To cancel the inherent interference, the real value of estimated symbol is taken before being demapped. Let $\tilde{\tilde{\mathbf{r}}}_k$ be the real signal at the input of the soft-demapper.

$\tilde{\tilde{r}}_k[l]$ denotes the lth stream of the kth carrier with $0 \leq l \leq N_T - 1$.

☐ Likelihood Bit Metrics

The receiver computes soft-decision metrics that are reliability quantifiers for each received bit. Then, for each received symbol $\tilde{\tilde{r}}_k[l]$, N metrics are computed (1 for each bit $b_k^i[l]$ with $i \in [0, N-1]$). The soft bit information assigned on bit $b_k^{I,i}[l]$, which is the Log-Likelihood Ratio (LLR) is defined by [TB02]

$$\text{LLR}(b_k^i[l]) = \log \frac{P[b_k^i[l] = 1 \mid \tilde{\tilde{r}}_k[l]]}{P[b_k^i[l] = 0 \mid \tilde{\tilde{r}}_k[l]]} \tag{5.41}$$

By assuming that the probability density functions are Gaussian and by considering the max-log approximation $(\log(\sum e^{x_i}) \approx \max(x_i))$[TB02] the expression can be simplified. This approximation yields as long as the sum is dominated by its largest term. Therefore, we obtain :

$$\text{LLR}(b_k^i[l]) \approx \frac{1}{2\sigma_k^2[l]} \left(\min_{\alpha \in S_i^{(0)}} \left| \tilde{\tilde{r}}_k[l] - \alpha \right|^2 - \min_{\alpha \in S_i^{(1)}} \left| \tilde{\tilde{r}}_k[l] - \alpha \right|^2 \right) \tag{5.42}$$

where $S_i^{(b)}$ represents the symbol set with a bit value 'b' (either 0 or 1) in position i. (5.42) is valid for both PPN and FS schemes.

☐ Linear Detection for PPN

Zero Forcing case

The Zero-Forcing equalization scheme processes the received vector by the pseudo-inverse of the channel matrix: $\mathbf{W}_{ZF,k} = (\mathbf{H}_k^H \mathbf{H}_k)^{-1} \mathbf{H}_k^H$ (for $k \in [0, M-1]$) where $(.)^H$ stands for the Hermitian transpose (assuming that $\mathbf{H}$ is well-conditioned). Applying the pseudo-inverse of $\mathbf{H}$ cancels all the ISI coming from others antennas (as $\mathbf{W}_{ZF}\mathbf{H} = \mathbf{I}_{N_T}$). Therefore, the symbols at the output of the equalizer are defined by

$$\tilde{r}_{ZF,k}[l] = a_k[l] + j u_k[l] + \tilde{n}_k[l] \tag{5.43}$$

with $\tilde{n}_k[l] \rightsquigarrow \mathcal{N}\left(0, \sum_{i=1}^{N_R} \mid (\mathbf{W}_{ZF,k})_{l,i} \mid^2 \sigma_n^2\right)$.

The conditional PDF of $\tilde{\tilde{r}}_{ZF,k}[l] = \Re(\tilde{r}_{ZF,k}[l])$ is thus normally distributed.

$$P[\tilde{\tilde{r}}_k[l] \mid a_k[l] = \alpha] = \frac{1}{\sqrt{2\pi\sigma_{\tilde{n}}^2/2}} \exp\left\{ -\frac{1}{2} \frac{\mid \tilde{\tilde{r}}_k[l] - \alpha \mid^2}{\sigma_{\tilde{n}}^2/2} \right\} \tag{5.44}$$

Therefore, the simplified LLRs for ZF equalization can be expressed as follows:

$$\text{LLR}(b_k^i[l]) = \frac{1}{\sigma^2_{\text{ZF},k}[l]} \left(\min_{\alpha \in S_i^{(0)}} \left| \tilde{\tilde{r}}_{ZF,k}[l] - \alpha \right|^2 - \min_{\alpha \in S_i^{(1)}} \left| \tilde{\tilde{r}}_{ZF,k}[l] - \alpha \right|^2 \right) \tag{5.45}$$

with

$$\sigma^2_{\text{ZF},k}[l] = \left(\sum_{i=1}^{N_R} \mid (\mathbf{W}_{ZF,k})_{l,i} \mid^2 \right) \sigma_n^2 \tag{5.46}$$

ZF scheme is convenient as it requires a simple LLR factor to be computed. However, the equalization scheme may suffer from noise enhancement.

MMSE case

The second equalization scheme is based on the Minimum Square-Error criterion. The MMSE criterion limits noise enhancement at the expense of a poorer Inter-Antenna Interference (IAI) cancellation. For PPN FBMC transmissions, two different expressions of the Mean Square Error can be of interest:

$$\underset{\mathbf{W}_k}{\text{argmin}} \left\{ E \left[|| \ \mathbf{W}_k(\mathbf{H}_k(\mathbf{a}_k + j\mathbf{u}_k) + \mathbf{n}_k) - (\mathbf{a}_k + j\mathbf{u}_k) \ ||^2 \right] \right\} \tag{5.47}$$

$$\underset{\mathbf{W}_k}{\text{argmin}} \left\{ E \left[|| \ \Re[\mathbf{W}_k(\mathbf{H}_k(\mathbf{a}_k + j\mathbf{u}_k) + \mathbf{n}_k)] - \mathbf{a}_k \ ||^2 \right] \right\} \tag{5.48}$$

The difference lies in the definition of the Mean Square Error: either a virtually transmitted symbol composed of the effective one and the inherent interference term is considered (5.47) [TJH07] or only the effective transmitted symbol with the projection on the real domain of the received and equalized symbol (5.48). It can be shown that, under the frequency flat channel per carrier condition, the two definitions lead to the same expression of $\mathbf{W}_{\text{MMSE}}$:

$$\mathbf{W}_{\text{MMSE},k} = (\mathbf{H}_k^H \mathbf{H}_k + \frac{\sigma_n^2}{2\sigma_a^2} \mathbf{I}_{N_T})^{-1} \mathbf{H}_k^H \tag{5.49}$$

In the MMSE case, residual Inter-Layer Interferences remain (as $\mathbf{W}_{\text{MMSE}}\mathbf{H}$ is not diagonal). It illustrates the trade-off operated by the MMSE equalizer between noise enhancement and IAI cancellation. This latter aspect makes the MMSE detector biased. It can also be noted that (5.49) matches with the OFDM expression of $\mathbf{W}_{\text{MMSE}}$.

The symbol (Ith stream and kth carrier) at the output of the equalizer can be expressed as

$$\tilde{\tilde{r}}_k[l] = \beta_{l,l}(a_k[l] + ju_k[l]) + \underbrace{\sum_{j \neq l} \beta_{l,j}(a_k[j] + ju_k[j]) + \tilde{n}_k[l]}_{\omega_k[l]} \tag{5.50}$$

where $\beta_{i,j} = (\mathbf{W}_{\text{MMSE}}\mathbf{H})_{i,j}$. $\tilde{n}_k[l]$ is the noise term with $\tilde{n}_k[l] = \left(\sum_{i=1}^{N_R} \mid (\mathbf{W}_{\text{MMSE}})_{l,i} \mid^2 \right) n_k[l]$. $\omega_k[l]$ is the interference plus noise term of the Ith stream. It can be approximated as a zero-mean Gaussian variable [KLP08]. Since $\beta_{l,l} \in]0,1[$ and is real-value [KLP08], the simplified LLR expression becomes

$$\text{LLR}(b_k^i[l]) = \frac{1}{\sigma^2_{\text{MMSE},k}[l]} \left(\min_{\alpha \in S_i^{(0)}} \left| \frac{\tilde{\tilde{r}}_k[l]}{\beta_l} - \alpha \right|^2 - \min_{\alpha \in S_i^{(1)}} \left| \frac{\tilde{\tilde{r}}_k[l]}{\beta_{l,l}} - \alpha \right|^2 \right) \tag{5.51}$$

with

$$\sigma^2_{\text{MMSE},k}[l] = \left(\sum_{j \neq l} \frac{\beta_{l,j}^2}{\beta_{l,l}^2} \right) \sigma_a^2 + \left(\sum_{i=1}^{N_R} \frac{\mid (\mathbf{W}_{\text{MMSE},k})_{l,i} \mid^2}{\beta_{l,l}^2} \right) \sigma_n^2 \tag{5.52}$$

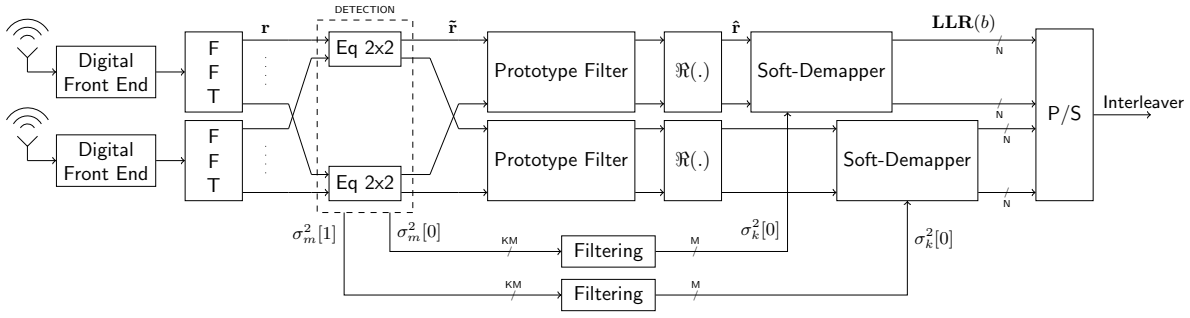

Figure 5-6: FS receiver structure with two reception antennas

☐ Linear Detection for FS

ZF case

The expression of $\mathbf{W}_{ZF}$ only depends on $\mathbf{H}$ and then does not differ from expressions introduced in the previous section. However, it is worth pointing out that its values are different as $\mathbf{H}$ is estimated for each subcarrier (frequency spacing of $\frac{1}{KM}$) and not for each carrier (frequency spacing of $\frac{1}{M}$) like for PPN.

$$\mathbf{W}_{\mathrm{ZF},m} = (\mathbf{H}_m^H \mathbf{H}_m)^{-1} \mathbf{H}_m^H \tag{5.53}$$

$$\sigma^2_{\mathrm{ZF,m}}[l] = \frac{1}{\sum_{i=1}^{N_R} \mid (\mathbf{W}_{\mathrm{ZF},m})_{l,i} \mid^2 \sigma_n^2} \tag{5.54}$$

MMSE

When it comes to the MMSE, we can use the same approach as for the PPN: considering a virtually symbol including the interference term $(\mathbf{b}_k + \mathbf{i}_k)$ (5.55).

$$\underset{\mathbf{W}_m}{\operatorname{argmin}} \left\{ E \left[|| \ \mathbf{W}_m(\mathbf{H}_m(\mathbf{b}_m + \mathbf{i}_m) + \mathbf{n}_m) - (\mathbf{b}_m + \mathbf{i}_m) \ ||^2 \right] \right\} \tag{5.55}$$

With the FS scheme, it is not possible to virtually remove the interference and thus to apply a solution similar to (5.48). Indeed, both the useful symbol term $\mathbf{b}_m$ and the interference term $\mathbf{i}_m$ are complex.

The FBMC filter design insures that $\sigma_b^2 = \sigma_a^2$ (using normalized filter shape) [Bel10](5.38). When it comes to the variance of the interference term, we have $\sigma_i^2 = \sigma_b^2$ like with the PPN. That is why $\mathbf{W}$ keeps the same expression as in (5.49). It is worth pointing out that, like the ZF case, the channel matrix $\mathbf{H}$ is defined at the subcarrier level for the FS and not at the carrier level like for the PPN.

$$\mathbf{W}_{\mathrm{MMSE},m} = (\mathbf{H}_m^H \mathbf{H}_m + \frac{\sigma_n^2}{2\sigma_a^2} \mathbf{I}_{N_T})^{-1} \mathbf{H}_m^H \tag{5.56}$$

$$\sigma^2_{\mathrm{MMSE,m}}[l] = \left(\sum_{j \neq l} \frac{\beta_{l,j}^2}{\beta_{l,l}^2} \right) \sigma_a^2 + \left(\sum_{i=1}^{N_R} \frac{|(\mathbf{W}_{\mathrm{MMSE},m})_{l,i}|^2}{\beta_{l,l}^2} \right) \sigma_n^2 \tag{5.57}$$

☐ LLR computation

The σ_m^2 given in (5.54) and (5.57) corresponds to the variance of the estimates determined at the subcarrier level (output of the detection stage). The objective now is to determine the variance of the estimates at the carrier level σ_k^2 which corresponds to the input of the

soft-demapper. With the Frequency-Spreading scheme, the symbols are spread over $2K-1$ consecutive subcarriers. During the over-the-air transmission, the $2K-1$ symbols are affected by different channel coefficients and at the receiver side they will be equalized independently. The estimated symbols $\tilde{\tilde{r}}_k[l]$ are determined through filtering. The variance σ_k^2 therefore corresponds to the variance of the linear combination of the subcarrier interference-plus-noise terms weighted by the filter coeffcients. The non-correlation of those terms is ensured by the independence of the subcarrier noise terms. Consequently, the expression of σ_k^2 can be simplified:

$$\sigma_{Eq,k}^2 = \sum_{m=kK}^{kK+2K-1} G_{m-kK}^2 \sigma_{Eq,m}^2[l] \tag{5.58}$$

where $Eq \in [ZF,$ MMSE$]$. A block diagram of the FS receiver is depicted in Fig 5-6. The LLR expression for the FS can thus be obtained by inserting (5.58) in (5.42).

5.3.2.4 Simulation results

In this section, the Bit Error Rate is evaluated for a 2×2 MIMO system. The overlapping factor of the PHYDYAS filter has been set to $K=4$. At the transmitted side, the data is encoded and processed through the convolutional encoder of rate $1/2$ and constraint length 7. The binary sequence is mapped to a QAM constellations (QPSK and 64-QAM). The LTE extended VehA [3GP12] channel model is used for the channel impulse responses which coefficients follow a Rayleigh distribution. The tap/delay table of the EVehA channel is depicted in Tab.5-2. The sampling frequency is set to 15.36 MHz. Two system configurations are assessed: 128-carrier system (Configuration 1) and 256-carrier system (Configuration 2). One can notice that the Configuration 1 is designed to suffer more from fast fading because of its larger inter-carrier spacing. On the contrary, as the duration of the symbol is decreased compared to configuration 1, configuration 2 is more robust to doppler shift. The BER at the output of the receiver is simulated by averaging 500 channel realizations. Simulation results for configurations 1 and 2 are respectively presented in Fig.5-7 and Fig.5-8.

Tap	1	2	3	4	5	6	7	8	9
Delay [ns]	0	30	150	310	370	710	1090	1730	2510
Power [dB]	0.0	-1.5	-1.4	-3.6	-0.6	-9.0	-7.0	12.0	16.9

Table 5-2: Multipath Profile of LTE Extended VehA Model

Observing the results, the FS scheme globally achieves better performances with both equalizer techniques (ZF and MMSE). Indeed for the PPN scheme, the variations of the channel at the carrier spacing level becomes appreciable and therefore the 1-tap equalizer does not fully compensate the channel effects. Therefore the orthogonality is not satisfied and the PPN exhibits an error floor due to the huge amount of residual interferences. On the contrary, the FS remains closer to the flat fading approximation thanks to its $(2K-1)$-tap equalization at the carrier level. The channel is better counteracted and the orthogonality is better satisfied. Consequently, the FS scheme outperforms the PPN.

As expected the MMSE equalizer performs better than the ZF thanks to its limited noise amplification. One can observe that the SNR gain provided by the FS scheme is slightly greater with the MMSE than with the ZF.

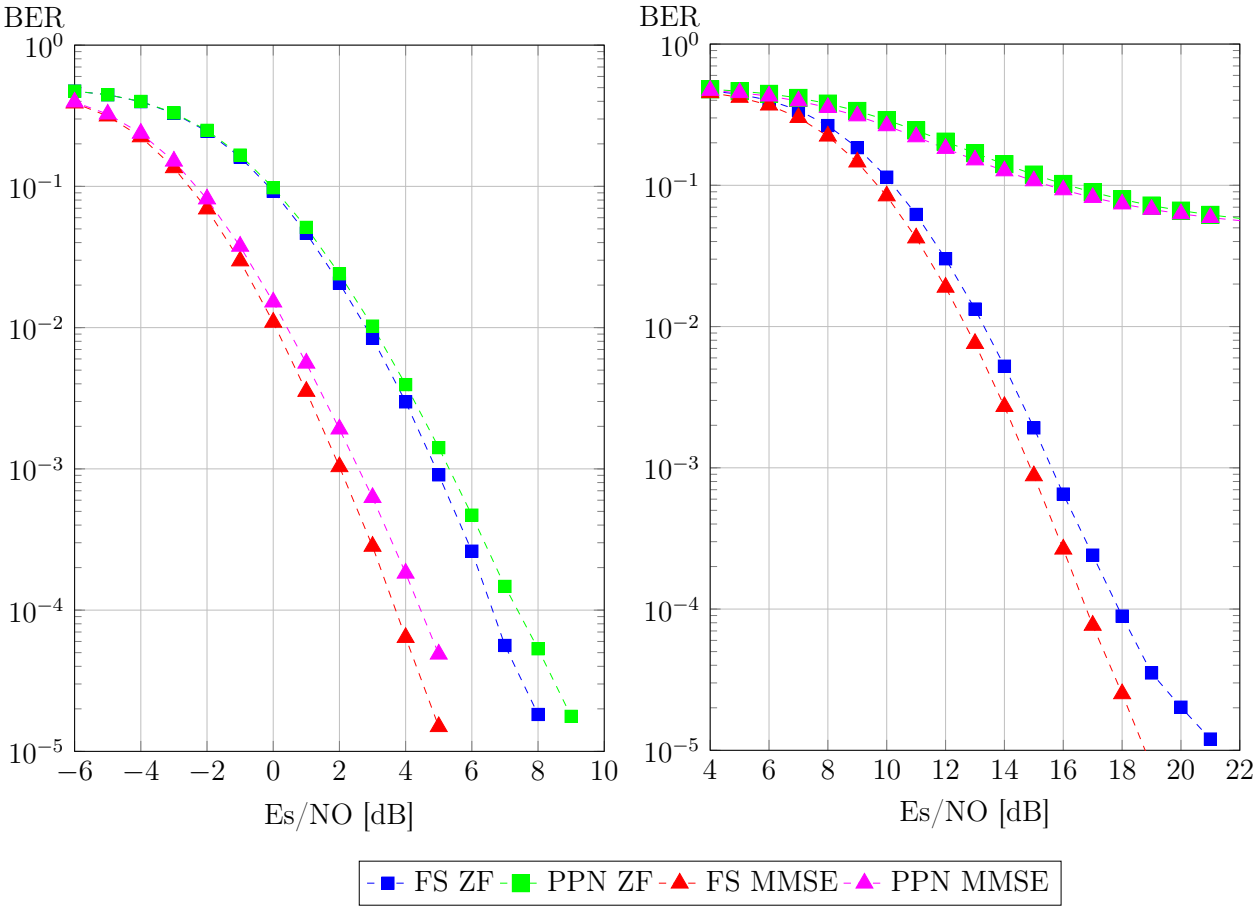

Figure 5-7: Performances for M=128 (QPSK top and 64-QAM bottom)

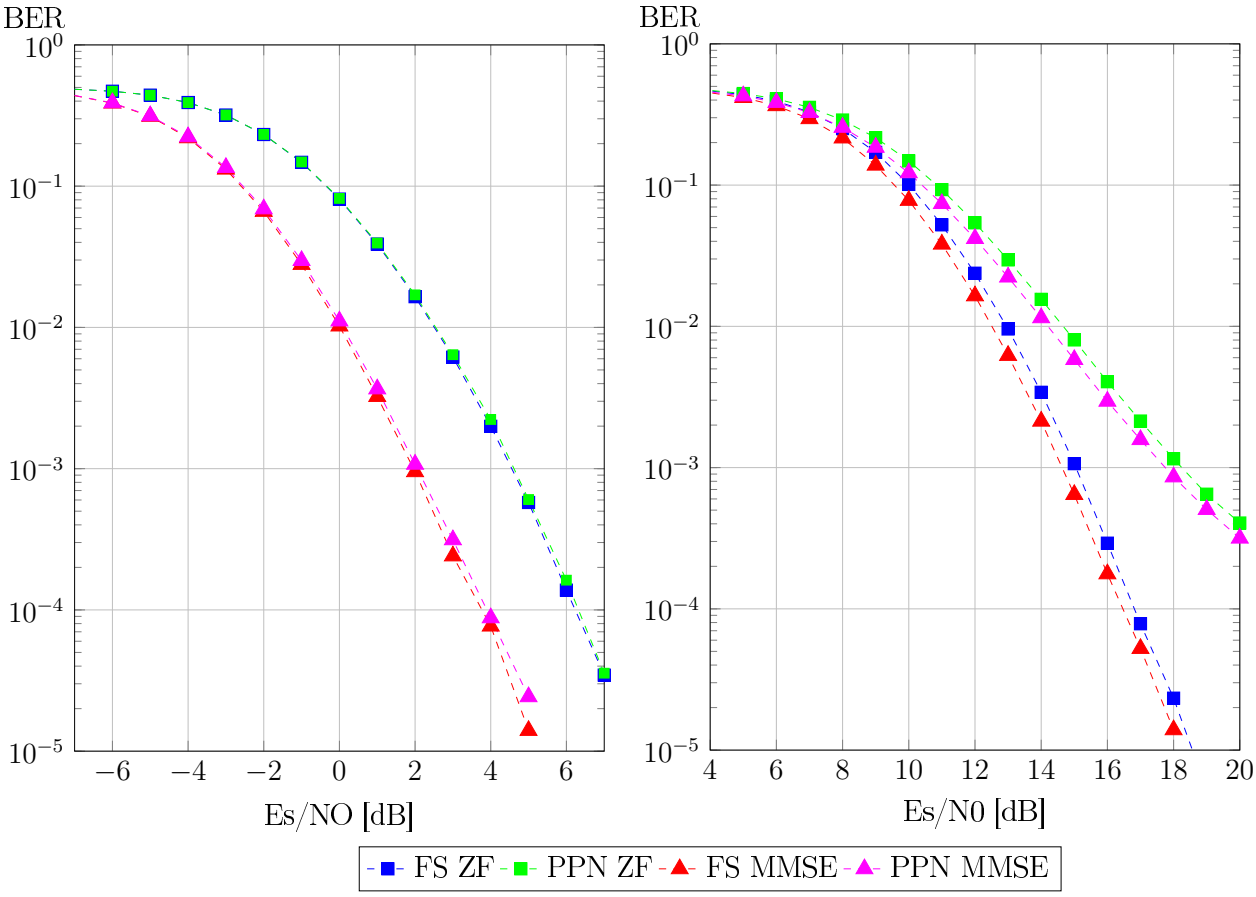

Figure 5-8: Performances for M=256 (QPSK top and 64-QAM bottom)

5.3.2.5 Conclusion

We have applied soft-input decoding to linear FBMC receivers and in particular to FS-FBMC receiver. The objective was to enhance the robustness the FBMC modulation to selective channels by improving the frequency resolution of the receiver. The FS scheme, with detection stage at the subcarrier level, performs a multi-tap equalization and therefore provides an appreciable SNR gain with respect to the PPN especially when the carrier spacing is larger than the coherence bandwidth of the channel. However, this scheme makes the channel estimation in pratice more complex as the channel should be estimated at the subcarrier level (with a frequency resolution of $\frac{1}{KM}$). This solution is not only interesting for high rate applications (with joint high number of carriers and large constellations) but also for cost-effective systems. Indeed, one can expect that it is possible to perform as well as a PPN receiver with K times less carrier by considering a FS receiver (same the frequency resolution). Reducing the number of carrier is a way to reduce the Peak-Power-to-Average Ratio and therefore to relax constraints on the efficiency enhancement techniques at the transmitter side.

5.3.3 Alamouti coding with FBMC/OQAM combined with Frequency Spreading receiver

In FBMC/OQAM, each subcarrier is filtered by a protype filter and is modulated with an Offset Quadrature Amplitude Modulation (OQAM). Real and imaginary symbols are transmitted with a delay corresponding to half the symbol period; consequently the orthogonality condition is only considered in the real field. At the receiver side, data symbols are carried by the real (resp. imaginary) component of the signal, whereas, the imaginary (resp. real) part is an inherent interference term. Alamouti coding intrinsically uses the complex orthogonality which makes its combination with FBMC not straightforward. In particular, the direct application of the well known Alamouti coding scheme [Ala98a] is not possible; the intrinsic interference breaks the orthogonality expected with Alamouti coding.

In [ZR13] the original Alamouti scheme is proposed for FBMC. The orthogonality of the the coding scheme is restored at the receiver by canceling the interference terms. The authors demonstrate that the receiver suffers from error propagation and the cancellation is not sufficiency effective to converge to performance offers by an Alamouti coded OFDM scheme.

In [LSL10] the authors prove that Alamouti coding can be performed when it is combined with a precoder (Walsh Hadamard codes). Full rate is achieved when particular subsets of precoders are combined and the complex orthogonality is preserved; complex symbols are sent and demodulated. However, interference appears between consecutive precoded symbols, making necessary the introduction of guard symbol(s), or making necessary to increase the size of the precoder. A similar approach was proposed in [ZLR10b]; the precoder is based on Fourier matrix coefficient (once again a subset of precoder has to be chosen carefully to guarantee the orthogonality). This scheme allows the transmission of complex symbols but needs the insertion of a cyclic prefix, reducing the overall efficiency.

In [RIS10], a block-wise Alamouti scheme is proposed. Such schemes have been initially applied in single-carrier [LP00] and in spread spectrum [MC05] transmission on channel with inter symbols interference. The orthogonality of the Alamouti coded frame is preserved by sending the conjugate time reverse block. In the basic scheme, guard times are inserted between the Alamouti coded frames to manage the interference. The performance of the block-wise Alamouti scheme combined with a PPN (poly phase network) based receiver is quite good in case of stationary channel with small frequency selectivity.

We propose to investigate how the block -wise Alamouti scheme and the Frequency-Spreading FBMC receiver can be adapted to improve performance in case of channel with high frequency selectivity.

5.4 Multi-Carriers approaches with linear receivers

The context is the multi-carriers transmission of FBMC-QAM. The main problem of such waveforms is the ISI/ICI interference between symbols and carriers respectively. For instance the ISI/ICI of the PHYDYAS[BLRR+10, Bel10] prototype filter are given in Table 5-1 where $r_m(kT)$ is the QAM symbol interference values of equations (5.20)(5.21) for $i = 2k$. According to Table 5-1 there is ICI without ISI for PHYDYAS. In section 5.1 the carrier per carrier MIMO receivers need interference cancelation for ISI/ICI.

Thus in this section, solutions associated to joint estimation of symbols on each carrier are proposed in order to take into account ISI/ICI modeling without processing interference cancelation. One of the advantage of these approaches is that all the energy associated to each symbol in the time and frequency domain is taking into account on receiver. The philosophy is given firstly in SISO/SIMO. Secondly the approach will be adapted to MIMO technology with STBC such as Alamouti [Ala98b] and V-BLAST[Fos96].

The purpose of FBMC multi-carrier waveforms is to transmit the time-frequency mapping $\{a_{mi}\}$ where m is the carrier index and i the time index of the complex symbol a_{mi}. The symbols mapping is transmitted with the following signal

$$s(t) = \sum_{m=0}^{M-1} \sum_i a_{mi} v_m (t - iT_s) \text{ with } \begin{cases} v_m(t) = v(t) \exp(j2\pi f_m t) \\ f_m = \Delta f \times m \text{ with } \Delta f = \frac{1}{T_s} \end{cases} \tag{5.59}$$

where T_s is the symbol duration and $v(t)$ is the pulse shaping filter. In SIMO context, the observation vector at the output of the receive antenna is given by

$$\mathbf{x}(t) = s(t) * \mathbf{h}(t) + \mathbf{n}(t) \tag{5.60}$$

where $\mathbf{h}(t)$ is the impulse response of the channel vector, $\mathbf{n}(t)$ is the additive noise and $*$ the convolution product. Assuming that the channel is flat on each carrier, the signal at the output of the $p-th$ carrier is

$$\begin{aligned} \mathbf{x}_p(t) &= v_p^*(-t) * \mathbf{x}(t) \\ &= \sum_{m=0}^{M-1} \sum_i a_{mi} \left[v_p^*(-t) * v_m(t - iT_s) * \mathbf{h}(t) \right] + \mathbf{n}_p(t) \\ &\approx \sum_{m=0}^{M-1} \sum_i \mathbf{h}_p \, a_{mi} \left[v_p^*(-t) * v_m(t - iT_s) \right] + \mathbf{n}_p(t) \end{aligned} \tag{5.61}$$

where $\mathbf{h}_p$ is the Fourier transform of $\mathbf{h}(t)$ at frequency f_p. Thus the discrete Fourier transform of $\mathbf{x}_p(t_i = i/(M\Delta f))$ gives

$$\mathbf{x}_p(f) \approx \sum_{m=0}^{M-1} \mathbf{h}_p \mathbf{a}_{[m]}(f) \mathbf{G}_{[p][m]}(f) + \mathbf{n}_p(f) \text{ with } \begin{cases} \mathbf{a}_{[m]}(f) = \sum_i a_{mi} \exp(-j2\pi f \times iT_s) \\ \mathbf{G}_{[p][m]}(f) = v_p^*(f) v_m(f) = \gamma_{m-n}(f) \\ \gamma_i(f) = v^*(f) v(f - f_i) \end{cases} \tag{5.62}$$

because $f_m - f_n = f_{m-n}$ according to (5.59) and also $\gamma_i(f) = \gamma_i(f - M\Delta f) = \gamma_{i-M}(f)$. Let's not that $\mathbf{G}_{[p][m]}(f)$ is the inverse Fourier transform of $r_{R,m,p}(t)$ in equation (5.20) when $R_B(f) = 1$ In presence of ICI, the components $\mathbf{G}_{[m][p]}(f)$ for $p \neq m$ are not null. The signal $\mathbf{x}_p(f)$ can be rewritten as

$$\mathbf{x}_p(f) \approx \mathbf{h}_p y_p(f) + \mathbf{n}_p(f) \tag{5.63}$$

$$y_p(f) = \sum_{m=0}^{M-1} \mathbf{G}_{[p][m]} \mathbf{a}_{[m]}(f) \tag{5.64}$$

where $y_p(f)$ is the signal of interest. In this preliminary work the equalization is considering in two steps. The first step is associated to channel equalization with the determination of $y_p(f)$ and the second step is associated to the carriers separation processing from the multi-carrier observation $\mathbf{z}(f) = [y_0(f) \cdots y_{M-1}(f)]^T$ and the particular algebraic structure of $\mathbf{G}$.

6. References

[3GP12] 3GPP. LTE; Evolved Universal Terrestrial Radio Access (E-UTRA); Base Station (BS) radio transmission and reception. TS 36.104 v.8.13.0 Release 8. Technical report, ETSI, 07-2012.

[AJM15] J. Abdoli, M. Jia, and J. Ma. Filtered ofdm: A new waveform for future wireless systems. In *2015 IEEE 16th International Workshop on Signal Processing Advances in Wireless Communications (SPAWC)*, pages 66–70, June 2015.

[Ala98a] S. Alamouti. A simple transmit diversity technique for wireless communications. *Selected Areas in Communications, IEEE Journal on*, 16(8):1451–1458, Oct 1998.

[Ala98b] S. M. Alamouti. A simple transmit diversity technique for wireless communications. *IEEE Journal on Selected Areas in Communications*, 16(8):1451–1458, Oct 1998.

[AM84] J. Anderson and S. Mohan. Sequential Coding Algorithms: A Survey and Cost Analysis. *Communications, IEEE Transactions on*, 32(2):169 – 176, feb 1984.

[AS97] O.E. Agazzi and N. Seshadri. On the use of tentative decisions to cancel intersymbol interference and nonlinear distortion (with application to magnetic recording channels). *Information Theory, IEEE Transactions on*, 43(2):394 –408, mar 1997.

[Bel08] M. Bellanger. Transmit diversity in multicarrier transmission using oqam modulation. In *Wireless Pervasive Computing, 2008. ISWPC 2008. 3rd International Symposium on*, pages 727–730, May 2008.

[Bel10] M Bellanger. FBMC physical layer: a primer. Technical report, ICT-PHYDYAS Project, 2010. available on http://www.ict-phydyas.org.

[Bel12a] M. Bellanger. FS-FBMC: A flexible robust scheme for efficient multicarrier broadband wireless access. In *Globecom Workshops, 2012 IEEE*, pages 192–196, Dec 2012.

[Bel12b] M. Bellanger. FS-FBMC: An alternative scheme for filter bank based multicarrier transmission. In *Communications Control and Signal Processing (ISCCSP),5th International Symposium on*, pages 1–4, May 2012.

[Bel12c] Maurice Bellanger. Fs-fbmc: A flexible robust scheme for efficient multicarrier broadband wireless access. In *Globecom Workshops (GC Wkshps), 2012 IEEE*, pages 192–196. IEEE, 2012.

[BLRR+10] M Bellanger, D Le Ruyet, D Roviras, M Terré, J Nossek, L Baltar, Q Bai, D Waldhauser, M Renfors, T Ihalainen, et al. Fbmc physical layer: a primer. *PHYDYAS, January*, 2010.

[BRV05] J. C. Belfiore, G. Rekaya, and E. Viterbo. The golden code: a 2 times;2 full-rate space-time code with nonvanishing determinants. *IEEE Transactions on Information Theory*, 51(4):1432–1436, April 2005.

[BT07] Norman C Beaulieu and Peng Tan. On the effects of receiver windowing on OFDM performance in the presence of carrier frequency offset. *IEEE Transactions on Wireless Communications*, 6(1):202–209, 2007.

[Cha66] RW Chang. High-speed multichannel data transmission with bandlimited orthogonal signals. *Bell Sys. Tech. J*, 45(10):1775–1796, 1966.

[CPNK14] Marius Caus, Ana I. Perez-Neira, and Adrian Kliks. Characterization of the effects of multi-tap filtering on FBMC/OQAM systems. *EURASIP Journal on Advances in Signal Processing*, 2014(1):1–15, 2014.

[CTB97] G. Caire, G. Taricco, and E. Biglieri. Bit-interleaved coded modulation. In *Proc. IEEE International Conference on Communications (ICC)*, pages 1463–1467 vol.3, Jun 1997.

[DBCK14] Jean-Baptiste Doré, Vincent Berg, Nicolas Cassiau, and Dimitri Kténas. FBMC receiver for multi-user asynchronous transmission on fragmented spectrum. *EURASIP Journal on Advances in Signal Processing*, 2014(1):1–20, 2014.

[DBK15] Jean-Baptiste Doré, Vincent Berg, and Dimitri Kténas. Channel estimation techniques for 5G cellular networks: FBMC and multiuser asynchronous fragmented spectrum scenario. *Trans. Emerging Tel. Tech.*, 26(1):15–30, 2015.

[DGD+17] David Demmer, Robin Gerzaguet, Jean-Baptiste Doré, Didier Le Ruyet, and Dimitri Kténas. Block-Filtered OFDM: an exhaustive waveform to overcome the stakes of future wireless technologies. In *submitted to IEEE ICC (ICC)*, Paris, France, May 2017.

[FBM16] B. Farhang-Boroujeny and H. Moradi. OFDM Inspired Waveforms for 5G. *IEEE Commun. Surveys Tutorials*, 18(4):2474–2492, 2016.

[Fos96] G. J. Foschini. Layered space-time architecture for wireless communication in a fading environment when using multi-element antennas. *Bell Labs Technical Journal*, 1(2):41–59, Autumn 1996.

[FS98] Hans Georg Feichtinger and Thomas Strohmer. *Gabor analysis and algorithms : theory and applications*. Applied and numerical harmonic analysis. BirkhÃ¤user, Boston, Mass., Basel, Berlin, 1998.

[GDDK17] Robin Gerzaguet, David Demmer, Jean-Baptiste Doré, and Dimitri Kténas. Block-Filtered OFDM: a new promising waveform for multi-service scenarios. In *submitted to IEEE ICC 2017 (ICC)*, Paris, France, May 2017.

[HiS16] Huawei HiSilicon. f-ofdm scheme and filter design. In *R1-165425*, May 2016.

[HtB03] B.M. Hochwald and S. ten Brink. Achieving near-capacity on a multiple-antenna channel. *Communications, IEEE Transactions on*, 51(3):389 – 399, march 2003.

[IL09] A. Ikhlef and J. Louveaux. Per subchannel equalization for mimo fbmc/oqam systems. In *2009 IEEE Pacific Rim Conference on Communications, Computers and Signal Processing*, pages 559–564, Aug 2009.

[KFL01] F. R. Kschischang, B. J. Frey, and H. A. Loeliger. Factor graphs and the sum-product algorithm. *IEEE Transactions on Information Theory*, 47(2):498–519, Feb 2001.

[KLP08] N. Kim, Y. Lee, and H. Park. Performance Analysis of MIMO System with Linear MMSE Receiver. *IEEE Transactions on Wireless Communications*, 7(11):4474–4478, November 2008.

[LFAB95] Bernard Le Floch, Michel Alard, and Claude Berrou. Coded orthogonal frequency division multiplex [tv broadcasting]. *Proceedings of the IEEE*, 83(6):982–996, 1995.

[LJL+07] C. Lélé, J.-P. Javaudin, R. Legouable, A. Skrzypczak, and P. Siohan. Channel estimation methods for preamble-based OFDM/OQAM modulations. In *in European Wireless, Paris, France*, Apr. 2007.

[LLS09] H. Lin, C. Lélé, and P. Siohan. A pseudo alamouti transceiver design for OFDM/OQAM modulation with cyclic prefix. In *Signal Processing Advances in Wireless Communications, 2009. SPAWC '09. IEEE 10th Workshop on*, pages 300 –304, june 2009.

[LP00] Erik Lindskog and A. Paulraj. A transmit diversity scheme for channels with intersymbol interference. In *Communications, 2000. ICC 2000. 2000 IEEE International Conference on*, volume 1, pages 307–311 vol.1, 2000.

[LRZ09] C. Lele, D. Le Ruyet, and R. Zakaria. On the decoding of single delay STTC using filter bank based multicarrier modulation. In *2009 6th International Symposium on Wireless Communication Systems*, pages 86–90, Sept 2009.

[LS08] H. Lin and P. Siohan. A new transceiver system for the OFDM/OQAM modulation with Cyclic Prefix. In *Personal, Indoor and Mobile Radio Communications, 2008. PIMRC 2008. IEEE 19th International Symposium on*, pages 1 –5, sept. 2008.

[LSL10] Chrislin Lélé, Pierre Siohan, and Rodolphe Legouable. The alamouti scheme with cdma-ofdm/oqam. *EURASIP J. Adv. Signal Process*, 2010:2:1–2:11, January 2010.

[LSLB] C. Lélé, P. Siohan, R. Legouable, and M Bellanger. CDMA transmission with complex OFDM/OQAM. *EURASIP Journal on Wireless Communications and Networking*, 2008.

[MC05] S. Mayrargue and T. Clessienne. Improved scheme of open loop transmit diversity (STTD) in the DS-CDMA case. In *International Workshop on Convergent Technologies (IWCT)*, June 2005.

[MSC12] J.P. Delmas MS. Sallem and P. Chevalier. Optimal SIMO MLSE receivers for the detection of linear modulation corrupted by noncircular interference. *IEEE workshop on Statistical Signal Processing (SSP'2012)*, pages 2630–2639, August 2012.

[MWG+02] B. Muquet, Zhengdao Wang, G. B. Giannakis, M. de Courville, and P. Duhamel. Cyclic prefixing or zero padding for wireless multicarrier transmissions? *IEEE Transactions on Communications*, 50(12):2136–2148, Dec 2002.

[PCa11] F. Dupuy P. Chevalier and. Widely Linear Alamouti Receivers for the Reception of Real-Valued signals corrupted by interferences. the alamouti SAIC/MAIC concept. *IEEE Trans. On Signal Processing*, 59(7):3339–3354, July 2011.

[PGNB04] A. J. Paulraj, D. A. Gore, R. U. Nabar, and H. Bolcskei. An overview of MIMO communications - a key to gigabit wireless. *Proceedings of the IEEE*, 92(2):198–218, Feb 2004.

[Qua] Qualcomm, Incorporated. R1-162199 - Waveform candidates.

[RIS10] M. Renfors, T. Ihalainen, and T.H. Stitz. A block-alamouti scheme for filter bank based multicarrier transmission. In *Wireless Conference (EW), 2010 European*, pages 1031–1037, April 2010.

[SKL16] D. Sim, K. Kim, and C. Lee. A layered detection algorithm based on interference cancellation for fbmc-qam. *IEEE Communications Letters*, 20(10):1939–1942, Oct 2016.

[SL17] D. Sim and C. Lee. A mimo receiver with two-dimensional ordering for maximum likelihood detection in fbmc-qam. *IEEE Communications Letters*, PP(99):1–1, 2017.

[SLW03] B. Steingrimsson, Zhi-Quan Luo, and Kon Max Wong. Soft quasi-maximum-likelihood detection for multiple-antenna wireless channels. *Signal Processing, IEEE Transactions on*, 51(11):2710 – 2719, nov 2003.

[SSL02] P. Siohan, C. Siclet, and N. Lacaille. Analysis and design of OFDM/OQAM systems based on filterbank theory. *IEEE Transactions on Signal Processing*, 50(5):1170–1183, May 2002.

[SW14] F. Schaich and T. Wild. Relaxed synchronization support of universal filtered multi-carrier including autonomous timing advance. In *2014 11th International Symposium on Wireless Communications Systems (ISWCS)*, pages 203–208, Aug 2014.

[TB02] F. Tosato and P. Bisaglia. Simplified soft-output demapper for binary interleaved COFDM with application to HIPERLAN/2. In *Proc. IEEE International Conference on Communications (ICC)*, volume 2, pages 664–668 vol.2, 2002.

[TJH07] M. El Tabach, J. P. Javaudin, and M. Helard. Spatial Data Multiplexing Over OFDM/OQAM Modulations. In *Proc. IEEE International Conference on Communications (ICC)*, pages 4201–4206, June 2007.

[TSC98] V. Tarokh, N. Seshadri, and A. R. Calderbank. Space-time codes for high data rate wireless communication: performance criterion and code construction. *IEEE Transactions on Information Theory*, 44(2):744–765, Mar 1998.

[Ung74] G. Ungerboeck. Adaptive Maximum Likelihood Receiver for Carrier-Modulated Data Transmission Systems. *IEEE Trans. Communications*, 22(5):624–636, May 1974.

[VBRB06] S. Van Beneden, J. Riani, and J.W.M. Bergmans. Cancellation of Linear Intersymbol Interference for Two-Dimensional Storage Systems. In *Communications, 2006. ICC '06. IEEE International Conference on*, volume 7, pages 3173 –3178, june 2006.

[VIS+09] Ari Viholainen, Tero Ihalainen, Tobias Hidalgo Stitz, Markku Renfors, and Maurice Bellanger. Prototype filter design for filter bank based multicarrier transmission. In *Signal Processing Conference, 2009 17th European*, pages 1359–1363. IEEE, 2009.

[VWS+13] V. Vakilian, T. Wild, F. Schaich, S. ten Brink, and J. F. Frigon. Universal-filtered multi-carrier technique for wireless systems beyond lte. In *2013 IEEE Globecom Workshops (GC Wkshps)*, pages 223–228, Dec 2013.

[WSC14] T. Wild, F. Schaich, and Y. Chen. 5g air interface design based on universal filtered (uf-)ofdm. In *2014 19th International Conference on Digital Signal Processing*, pages 699–704, Aug 2014.

[WWS15] X. Wang, T. Wild, and F. Schaich. Filter optimization for carrier-frequency- and timing-offset in universal filtered multi-carrier systems. In *2015 IEEE 81st Vehicular Technology Conference (VTC Spring)*, pages 1–6, May 2015.

[WWSdS14] X. Wang, T. Wild, F. Schaich, and A. Fonseca dos Santos. Universal filtered multi-carrier with leakage-based filter optimization. In *European Wireless 2014; 20th European Wireless Conference*, pages 1–5, May 2014.

[YKK+15] Yeo Hun Yun, Chanhong Kim, Kyeongyeon Kim, Zuleita Ho, Byunghwan Lee, and Ji-Yun Seol. A new waveform enabling enhanced qam-fbmc systems. In *Signal Processing Advances in Wireless Communications (SPAWC), 2015 IEEE 16th International Workshop on*, pages 116–120. IEEE, 2015.

[Zak12] Rostom Zakaria. *Transmitter and receiver design for inherent interference cancellation in MIMO filter-bank based multicarrier systems*. Theses, Conservatoire national des arts et metiers - CNAM, November 2012.

[ZLR10a] R. Zakaria and D. Le Ruyet. A novel FBMC scheme for Spatial Multiplexing with Maximum Likelihood detection. In *Wireless Communication Systems (ISWCS), 2010 7th International Symposium on*, pages 461 –465, sept. 2010.

[ZLR10b] R. Zakaria and D. Le Ruyet. A novel fbmc scheme for spatial multiplexing with maximum likelihood detection. In *Wireless Communication Systems (ISWCS), 2010 7th International Symposium on*, pages 461–465, Sept 2010.

[ZLR11a] R. Zakaria and D. Le Ruyet. On spatial data multiplexing over coded filter-bank multicarrier with ML detection. In *Personal Indoor and Mobile Radio Communications (PIMRC), 2011 IEEE 22nd International Symposium on*, pages 1391 –1395, sept. 2011.

[ZLR11b] R. Zakaria and D. Le Ruyet. Partial ISI cancellation with viterbi detection in MIMO filter-bank multicarrier modulation. In *Wireless Communication Systems (ISWCS), 2011 8th International Symposium on*, pages 322 –326, nov. 2011.

[ZLR16] Rostom Zakaria and Didier Le Ruyet. Partial interference cancellation with maximum likelihood sequence detection in fbmc spatial multiplexing system. *EURASIP Journal on Advances in Signal Processing*, 2016(1):47, 2016.

[ZLRB10] R. Zakaria, D. Le Ruyet, and M. Bellanger. Maximum likelihood detection in spatial multiplexing with FBMC. In *Wireless Conference (EW), 2010 European*, pages 1038 –1041, april 2010.

[ZLRM12] R. Zakaria, D. Le Ruyet, and Y. Medjahdi. On ISI cancellation in MIMO-ML detection using FBMC/QAM modulation. In *Wireless Communication Systems (ISWCS), 2012 International Symposium on*, pages 949 –953, aug. 2012.

[ZMSR16] R. Zayani, Y. Medjahdi, H. Shaiek, and D. Roviras. WOLA-OFDM: a potential candidate for asynchronous 5G. In *IEEE Global Communications Conference (GLOBECOM)*, 2016.

[ZR12] R. Zakaria and D. Le Ruyet. A Novel Filter-Bank Multicarrier Scheme to Mitigate the Intrinsic Interference: Application to MIMO Systems. *IEEE Transactions on Wireless Communications*, 11(3):1112–1123, March 2012.

[ZR13] R. Zakaria and D.Le Ruyet. On interference cancellation in alamouti coding scheme for filter bank based multicarrier systems. In *Wireless Communication Systems (ISWCS 2013), Proceedings of the Tenth International Symposium on*, pages 1–5, Aug 2013.

[ZR14] Rostom Zakaria and Didier Le Ruyet. Intrinsic interference reduction in a filter bank-based multicarrier using QAM modulation . *Physical Communication*, 11:15–24, 2014. Radio Access Beyond OFDM(A).

[ZR16] R. Zakaria and D. Le Ruyet. FFT-FBMC equalization in selective channels. *Submitted to IEEE Signal Processing Letters*, 2016.

Glossary and Definitions

Acronym	Meaning
ACL	Adjacent Channel Leakage
C-MTC	Critical-Machine Type Communications
CCDF	Complementary Cumulative Distribution Function
COQAM	Circular Offset QAM
CFO	Carrier Frequency Offset
CP	Cyclic Prefix
EVM	Error Vector Magnitude
FBMC	Filter Bank Multi-Carrier
FFT	Fast Fourier Transform
FMT	Filtered Multi-Tone
f-OFDM	filtered-OFDM
FS	Frequency Spreading
GFDM	Generalized Frequency Division Multiplexing
IAPR	Instantaneous-to-Average Power Ratio
LTE	Long Term Evolution
MF	Matched Filter
MIMO	Multi-Input Multi-Output
MSE	Mean Square Error
OFDM	Orthogonal Frequency Division Multiplexing
OLA	Overlap and Add
OLS	Overlap and Save
OOB	Out-Of-Band
PAPR	Peak-to-Average Power Ratio
PPN	Poly-Phase Network
PSD	Power Spectral Density
RB	Resource Block
RRC	Root Raised-Cosine
Rx-W-OFDM	CP-OFDM with receive windowing
Tx-W-OFDM	CP-OFDM with transmit windowing
UFMC (i.e. UF-OFDM)	Universal-Filtered Multi-Carrier (i.e. Universal-Filtered OFDM)
UOI	User Of Interest
WCP	Windowed Cyclic Prefix
WF	WaveForm
WOLA	Weighted Overlap and Add
ZP	Zero Padding